Molecular Cancer

RESEARCH

Open Access

Cell-autonomous IL6ST activation suppresses prostate cancer development via STAT3/ARF/p53-driven senescence and confers an immune-active tumor microenvironment

Christina Sternberg[1,2,3*], Martin Raigel[1,3,4], Tanja Limberger[1,4,5], Karolína Trachtová[4,6], Michaela Schlederer[1], Desiree Lindner[3], Petra Kodajova[3], Jiaye Yang[1], Roman Ziegler[3,17], Jessica Kalla[1], Stefan Stoiber[1,4,7], Saptaswa Dey[8], Daniela Zwolanek[9], Heidi A. Neubauer[10,18], Monika Oberhuber[5], Torben Redmer[3], Václav Hejret[6], Boris Tichy[6], Martina Tomberger[5], Nora S. Harbusch[5], Jan Pencik[1], Simone Tangermann[3], Vojtech Bystry[6], Jenny L. Persson[11,12], Gerda Egger[1,13], Sarka Pospisilova[6], Robert Eferl[9], Peter Wolf[8,14], Felix Sternberg[15,16], Sandra Högler[3], Sabine Lagger[3], Stefan Rose-John[2*†] and Lukas Kenner[1,3,5,7,13*†]

Abstract

Background Prostate cancer ranks as the second most frequently diagnosed cancer in men worldwide. Recent research highlights the crucial roles IL6ST-mediated signaling pathways play in the development and progression of various cancers, particularly through hyperactivated STAT3 signaling. However, the molecular programs mediated by IL6ST/STAT3 in prostate cancer are poorly understood.

Methods To investigate the role of IL6ST signaling, we constitutively activated IL6ST signaling in the prostate epithelium of a *Pten*-deficient prostate cancer mouse model in vivo and examined IL6ST expression in large cohorts of prostate cancer patients. We complemented these data with in-depth transcriptomic and multiplex histopathological analyses.

Results Genetic cell-autonomous activation of the IL6ST receptor in prostate epithelial cells triggers active STAT3 signaling and significantly reduces tumor growth in vivo. Mechanistically, genetic activation of IL6ST signaling mediates senescence via the STAT3/ARF/p53 axis and recruitment of cytotoxic T-cells, ultimately impeding tumor progression. In prostate cancer patients, high *IL6ST* mRNA expression levels correlate with better recurrence-free survival, increased senescence signals and a transition from an immune-cold to an immune-hot tumor.

†Stefan Rose-John and Lukas Kenner co-last authors.

*Correspondence:
Christina Sternberg
christina.sternberg@meduniwien.ac.at
Stefan Rose-John
rosejohn@biochem.uni-kiel.de
Lukas Kenner
lukas.kenner@meduniwien.ac.at
Full list of author information is available at the end of the article

© The Author(s) 2024. **Open Access** This article is licensed under a Creative Commons Attribution-NonCommercial-NoDerivatives 4.0 International License, which permits any non-commercial use, sharing, distribution and reproduction in any medium or format, as long as you give appropriate credit to the original author(s) and the source, provide a link to the Creative Commons licence, and indicate if you modified the licensed material. You do not have permission under this licence to share adapted material derived from this article or parts of it. The images or other third party material in this article are included in the article's Creative Commons licence, unless indicated otherwise in a credit line to the material. If material is not included in the article's Creative Commons licence and your intended use is not permitted by statutory regulation or exceeds the permitted use, you will need to obtain permission directly from the copyright holder. To view a copy of this licence, visit http://creativecommons.org/licenses/by-nc-nd/4.0/.

Conclusions Our findings demonstrate a context-dependent role of IL6ST/STAT3 in carcinogenesis and a tumor-suppressive function in prostate cancer development by inducing senescence and immune cell attraction. We challenge the prevailing concept of blocking IL6ST/STAT3 signaling as a functional prostate cancer treatment and instead propose cell-autonomous IL6ST activation as a novel therapeutic strategy.

Keywords Prostate cancer, IL6ST/STAT3 signaling, L-gp130, Senescence, Senescence-associated secretory phenotype, Tumor microenvironment, Immune cell infiltration, Cytotoxic T-cells

Background

Prostate cancer (PCa) is the second most common cancer type diagnosed in men, as reflected by 1.4 million new cases worldwide and 375,000 related deaths in 2020 alone [1]. Corresponding to the vast PCa heterogeneity regarding clinical and molecular features, a wide range of therapeutic approaches is currently in use. The accuracy of these treatments is often hampered by the lack of reliable biomarkers allowing to distinguish aggressive from non-aggressive tumors [2]. In search of such biomarkers, aberrant activity of the Interleukin-6 cytokine family signal transducer (IL6ST), also known as Glycoprotein 130 kDa (GP130), signaling axis has been identified as a crucial factor in inflammation and carcinogenesis [3, 4]. A key downstream mediator of IL6ST signaling is the transcription factor Signal transducer and activator of transcription 3 (STAT3) [3]. STAT3 signaling is aberrant in approximately 50% of PCa [5] and plays a tumor microenvironment (TME)-dependent role in cell proliferation, cell survival, angiogenesis and immune evasion [6–8]. Therefore, a further characterization of the axis connecting IL6ST and STAT3 or other potential downstream targets in PCa is important for improved treatment approaches. Other targets activated by IL6ST include the Src homology 2 domain-containing tyrosine phosphatase-2 (SHP2), Phosphatidylinositol 3-kinase (PI3K) and the Hippo/YES-associated protein (YAP) pathway [9], which have themselves been linked with PCa [10–12]. Similarly, the tumor suppressor Phosphatase and tensin homolog (PTEN) is frequently mutated or deleted in PCa [13], thereby eliciting aberrant PI3K activation, contributing to prostate carcinogenesis [14] and inducing p53-dependent cellular senescence [15]. Senescence is a state of cell cycle arrest mediated by the $p19^{ARF}$/p53 or $p16^{INK4A}$/RB pathway and has been shown to inhibit PCa progression [16]. Senescence is often accompanied by the release of inflammatory cytokines, chemokines, growth factors and proteases, referred to as the senescence-associated secretory phenotype (SASP) [17]. The SASP is a double-edged sword exerting tumor-suppressive and tumor-promoting effects. The factors modulating the balance between pro-tumorigenic and anti-tumorigenic senescence effects are likely cell type-specific and not fully understood [18].

To shed new light on the role of IL6ST signaling in PCa pathogenesis and to gain further insight into the complex downstream signaling network, we created a mouse model featuring constitutive, cell-autonomous, and prostate epithelium-specific activation of IL6ST. Utilizing this model, we aimed at identifying molecular players induced by IL6ST signaling and at determining its importance in PCa initiation and progression. Considering recent endeavors to render immune-cold PCa amenable to anti-tumor immunity [19], our study also aimed to elucidate the role of IL6ST signaling in shaping the TME, thereby providing valuable insights into its potential use for therapeutic and diagnostic strategies for PCa management.

Our data show that constitutively active IL6ST signaling in *Pten*-deficient PCa mice is associated with significantly smaller tumors compared with *Pten*-deficient mice, related with IL6ST-induced activation of the STAT3/$p19^{ARF}$/p53 tumor suppressor axis mediating senescence. This is accompanied by increased infiltration of cytotoxic T-cells, neutrophils, and macrophages, indicating better anti-tumor defense. These findings are supported by improved survival observed in PCa patients showing high *IL6ST* mRNA expression, active senescence patterns, and a T-cell mediated anti-tumor immune defense. Together, these results highlight a context-dependent, tumor-suppressive role of IL6ST/STAT3 signaling in prostate carcinogenesis and suggest that cell-autonomous IL6ST activation may be a promising novel therapeutic approach for the treatment of PCa.

Methods

Generation of transgenic mice

Pten$^{fl/fl}$ [20], *L-gp130*$^{fl/fl}$ [3] and PB-Cre4 [21] transgenic mice were maintained on a C57BL/6 and Sv/129 mixed genetic background. *Pten*$^{fl/fl}$ mice and/or *L-gp130*$^{fl/fl}$ mice were crossed with male PB-Cre4 transgenic mice to generate prostate-specific deletion of *Pten* and/or insertion of the *L-gp130* construct. DNA isolation was performed as previously described [22]. Mice were genotyped as previously described [3, 20, 21, 23]. Mice were housed on a 12–12 light cycle and provided food and water ad libitum. For all experiments, 19-week old male mice

were used. Genotyping primer sequences and protocols are listed in Supplementary Table 1–2, Additional File 1. Formalin-fixed paraffin-embedded (FFPE) prostate tissue from *Pten*$^{pe\Delta/\Delta}$;*Stat3*$^{pe\Delta/\Delta}$ and respective *Pten*$^{pe\Delta/\Delta}$ control mice were provided by Pencik et al. [8].

Immunohistochemistry (IHC) and hematoxylin & eosin (H&E) stains

IHC and H&E stains were performed with FFPE prostate tissue using standard protocols and antibodies listed in Supplementary Table 3, Additional File 1.

Immunofluorescence (IF) staining

Frozen tissue sections were fixed with 4% Formol for 15 min at room temperature. After washing with PBS, tissue was blocked with 2% BSA in PBS prior to overnight primary antibody incubation at 4 °C (Supplementary Table 3, Additional File 1). Secondary antibody incubation (Alexa Fluor 594 anti-rabbit, Invitrogen #A11037, 1:500; RRID:AB_2534095) was done in 2% BSA in PBS for 1 h at room temperature. Cells were counterstained with DAPI (nuclear stain) in PBS and mounted with Aqua-Poly/Mount medium (18,606–5, Polysciences).

Multiplex IHC

Multiplex IHC was performed on mouse prostate samples using the Bond RX autostainer system (Leica Biosystems Inc., Vienna, Austria; RRID:SCR_025548) and were subsequently analyzed by multispectral imaging. A panel of the following fluorescent markers plus DAPI as a nuclear stain were used to detect the following epitopes: CD3, CD4, CD8, CD45, pan Cytokeratin (Supplementary Table 3, Additional File 1). Scanning of multiplex IHC stains was done as previously described [24]. Individual cells were detected using DAPI nucleus staining by applying thresholds for nucleus size, roundness, and signal intensity. Positivity thresholds for the fluorescently labeled markers were determined based on staining intensity.

Histopathological analysis

For histopathological analysis of H&E, IHC or IF stained samples, slides were scanned using a PANNORAMIC Scan II from 3DHISTECH and quantitatively analyzed as previously described [24]. The murine prostate consists of four different lobes: the anterior, ventral, lateral, and dorsal prostate, each exhibiting distinct morphological characteristics. Due to the loss of these characteristics during tumor progression, differentiating between the lobes in tumor tissue is only feasible for the spatially separated anterior prostate. Therefore, we classified the tissue into two regions: the "anterior lobe (AL)" and the "caudal lobe (CL)", which comprises the ventral, lateral, and dorsal prostate. These stratified data are presented in Additional File 2 and Additional File 3. In the main and supplementary figures, we show analyses covering the entire prostate except for F4/80 and NimpR14 analyses. For these, only the CL was used, as the lumen of the AL contains more cellular debris, which leads to nonspecific staining and challenges analysis. Cell detection was carried out using the StarDist [25] extension for NimpR14 staining, while the built-in watershed cell detection plugin was employed for the other stainings. Parameters were tailored for each specific staining. Subsequently, smoothed features were calculated using a full width at half maximum (FWHM) radius of 25 µm. The tissue was then classified into epithelium and stroma through an object classifier, trained individually for each staining. A threshold was set for the mean DAB optical density value to categorize cells as either positive or negative. If automated quantification was not possible for IHC stainings, semi-quantitative analysis was performed by a trained pathologist, who classified the level of expression as none, mild, moderate or marked for each tissue section. A similar approach was taken for the grading of immune cell infiltration, which was classified as low or high in H&E-stained sections. Analyses were performed blinded to genotype by a single investigator and evaluated by two independent pathologists with specific expertise in mouse models of PCa. A whole slide scan of stained prostate tissue per mouse was analyzed. Representative pictures of the CL for the main and supplementary figures, as well as representative pictures of the AL (and CL) for Additional File 2 and Additional File 3 were exported from whole slide scan using the snapshot function of CaseViewer (Build 2.4.0.119028; RRID:SCR_017654).

Protein isolation and immunoblotting

Whole prostate protein lysates were extracted from snap frozen prostate samples as described [26] and 20–40 µg of protein lysate was used for Western blotting as previously described [8]. Chemiluminescent visualization was performed with a ChemiDoc™ Imaging System (Bio-Rad; RRID:SCR_019037) after incubation of the membranes with Clarity Western ECL reagent (Bio-Rad, 170–5061). Near-infrared visualization was performed using an Odyssey Classic Imaging System (LI-COR; RRID:SCR_023765) and IRDye fluorescent secondary antibodies. Quantifications were performed with Image Lab software (Bio-Rad; RRID:SCR_014210). Samples were normalized to the indicated loading controls. Applied antibodies are listed in Supplementary Table 3, Additional File 1.

RNA sequencing (RNA-Seq) and data analysis

RNA-Seq sample and library preparation was performed as described in [22]. Briefly, single cell suspension of mouse prostate tissue was done as previously described [27] and magnetic cell separation (MagniSort technology, Thermo Fisher) was performed for EpCAM positive fraction using anti-mouse CD326 (EpCAM) Biotin antibody (13–5791-82, eBioscience; RRID:AB_1659713). For higher RNA output, three wild type and three *L-gp130*$^{peKI/KI}$ mouse prostates, respectively, were pooled to generate one sample. High-quality RNA was used for library preparation. Libraries were amplified with 11 PCR cycles and the library size was analyzed by Agilent Tape Station (G2938-90,014, Agilent Technologies). RNA sequencing and bioinformatic analysis of mouse prostate samples up to the differential expression was performed by Core Facility Bioinformatics of CEITEC Masaryk University as previously described [22].

The Cancer Genome Atlas (TCGA) data analysis

Clinical data for the TCGA-Prostate Adenocarcinoma (PRAD) cohort (https://portal.gdc.cancer.gov/projects/TCGA-PRAD) [28], including disease-free survival, were downloaded from the cBioPortal [29, 30] database. Raw expression counts were downloaded from TCGA with the TCGAbiolinks R package (version 2.25.3). Patients with mutation in TP53 gene (Supplementary Table 4, Additional File 1) were removed from subsequent analysis for Fig. 6b-c. Raw counts were transformed with the variance stabilizing transformation (VST). Survival analysis of TCGA-PRAD cohort was performed with the survminer R package [31] (version 0.4.9). Patients were divided into *IL6ST*$^{high/low}$ expression groups based on the maximally selected rank statistics which provides a single value cutpoint that corresponds to the most significant relation with disease-free survival. Differential expression analysis between *IL6ST*^{high} and *IL6ST*^{low} group was performed with DESeq2 (version 1.36.0). Alteration data including frequency of specific mutations and correlation analysis were obtained from the cBioPortal [29, 30] database. Immune scores for TCGA-PRAD cohort from the ESTIMATE method [32] were downloaded from https://bioinformatics.mdanderson.org/estimate/. Using the Mann–Whitney test, we assessed whether there was a statistically significant difference in the immune scores between *IL6ST*^{high} and *IL6ST*^{low}.

Statistical analysis

Significant differences between two groups were determined using a two-tailed, unpaired t-test (parametric) or Mann–Whitney test (non-parametric). Significant differences between more than two groups were determined using One-way ANOVA with Tukey's multiple comparison test (parametric). Significant outliers were identified by Grubbs ' test. p values of < 0.05 were assigned significance. All values are given as means ± standard deviation (SD) and were analyzed and plotted by GraphPad Prism® (version 9.5.0, GraphPad Software, San Diego, CA). Numbers of biological replicates are stated in the respective figure legends. The associations between genes/gene sets and their respective statistical significances were assessed using Spearman-correlation.

Additional methods can be found in Supplementary Methods, Additional File 4.

(See figure on next page.)

Fig. 1 Prostate epithelium-specific, cell-autonomous insertion of *L-gp130* reduces progressive prostate tumorigenesis. **a** Illustration of wild type IL6ST receptor, which can be activated by binding of the IL-6 ligand and IL-6R receptor (left panel), and Leucine-gp130 (L-gp130) construct (right panel). Wild type IL6ST consists of an extracellular domain comprising an Ig-like domain, a cytokine binding domain, three fibronectin type III-like domains, a transmembrane domain, and a cytoplasmic domain. For generating L-gp130, wild type IL6ST was truncated 15 amino acids above the transmembrane domain and replaced by the leucine zipper region of the human c-JUN gene and a FLAG-Tag. L-gp130 expression can activate downstream signaling cascades identical to stimulated wild type IL6ST. P: phosphorylation. **b** Illustration of the genetic approach for conditional deletion of *Pten* (exon 4 + 5) or/and insertion of *L-gp130-ZSGreen* in prostate epithelial cells under the control of Probasin (PB) promoter after *Cre*-mediated recombination resulting in PB-Cre4;*Pten*$^{fl/fl}$;*L-gp130*$^{+/+}$ (hereafter *Pten*$^{peΔ/Δ}$), PB-Cre4;*Pten*$^{+/+}$;*L-gp130*$^{fl/fl}$ (hereafter *L-gp130*$^{peKI/KI}$) and PB-Cre4;*Pten*$^{fl/fl}$;*L-gp130*$^{fl/fl}$ mice (hereafter *Pten*$^{peΔ/Δ}$;*L-gp130*$^{peKI/KI}$). pe: prostate epithelium; fl: floxed site; ex: exon; 2A: 2A peptide; CAG: CAG promoter; KI: knock in; Δ: knock out. **c** Representative immunohistochemistry (IHC) pictures of phospho-AKT (p-AKT) and immunofluorescence (IF) pictures of co-stainings of ZSGreen (red) and DAPI (blue) in mouse prostates. DAPI is used as a nuclear stain. Scale bar: 40 µm. Scale bar of inset: 10 µm. **d** Gross anatomy of representative mouse prostates. Scale bar: 0.5 cm. **e** Prostate weight of wild type ($n = 10$), *L-gp130*$^{peKI/KI}$ ($n = 14$), *Pten*$^{peΔ/Δ}$ ($n = 14$), and *Pten*$^{peΔ/Δ}$;*L-gp130*$^{peKI/KI}$ ($n = 14$) mice. Individual biological replicates are shown. Data are plotted as the means ± SD and p-values were determined by ordinary one-way ANOVA with Tukey's multiple comparisons test. **f** Representative pictures of hematoxylin & eosin (H&E) stains of mouse prostates at low (top) and high (bottom) magnification. Scale bar upper panel: 60 µm, scale bar lower panel: 10 µm. **g** Quantification of histopathological analysis of prostate tissue from wild type ($n = 9$), *L-gp130*$^{peKI/KI}$ ($n = 9$), *Pten*$^{peΔ/Δ}$ ($n = 11$), and *Pten*$^{peΔ/Δ}$;*L-gp130*$^{peKI/KI}$ ($n = 9$) mice in regards of histomorphological criteria for aggressive growth patterns: without pathological findings (white); PIN: prostate intraepithelial neoplasia (grey); PCa: prostate cancer (red)

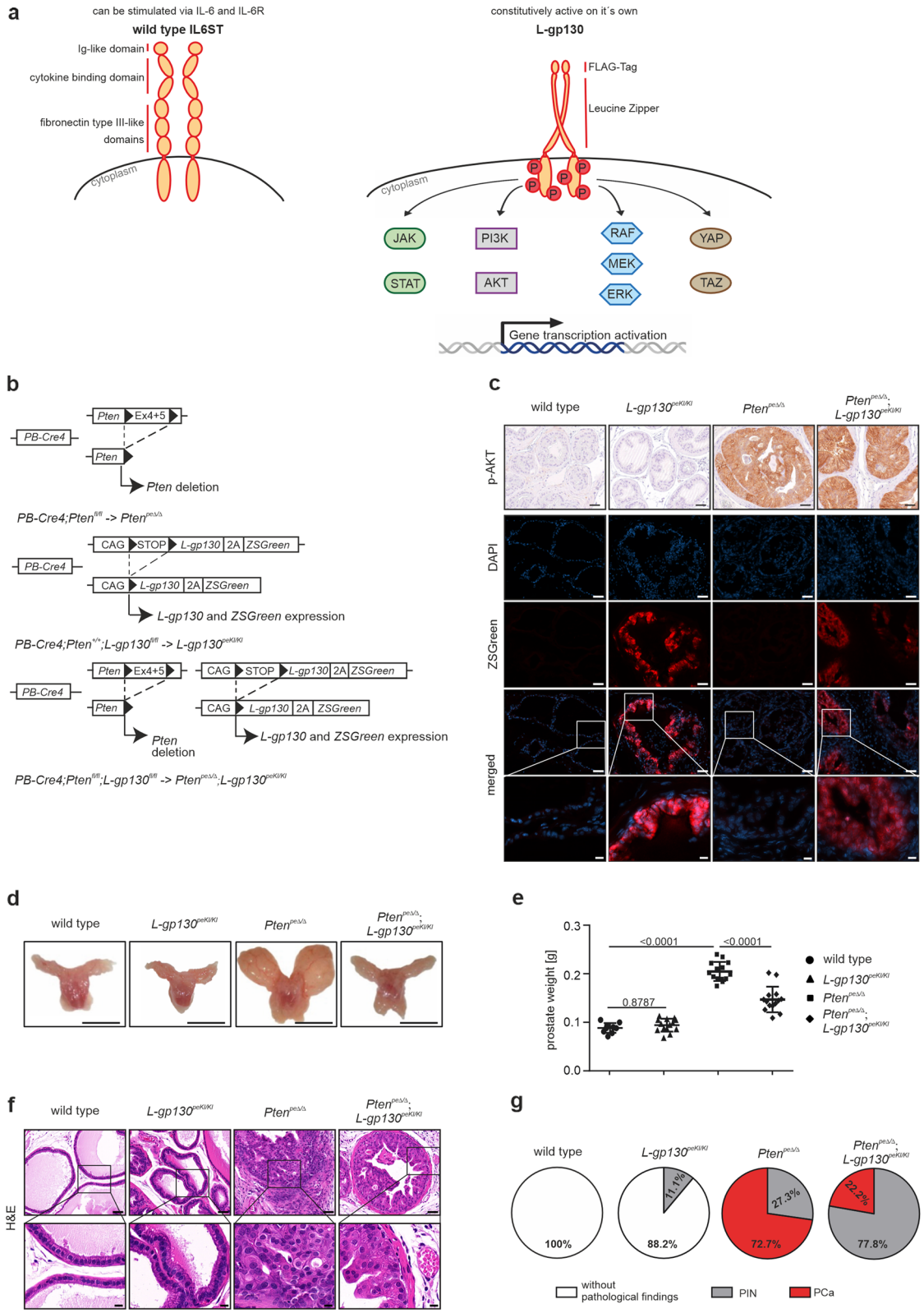

Fig. 1 (See legend on previous page.)

Results

Constitutive activation of IL6ST signaling in prostate epithelial cells

To investigate constitutively activated IL6ST signaling, we used the so-called Leucine-gp130 (L-gp130) construct introduced by Stuhlman-Laeisz et al. [33] (Fig. 1a, right panel), where the entire extracellular part of the wild type IL6ST receptor (Fig. 1a, left panel) is replaced by a leucine zipper, causing forced receptor dimerization and ligand-independent constitutive activation of downstream signaling. The wild type IL6ST receptor requires stimulation by the cytokine Interleukin-6 (IL-6) and Interleukin-6 receptor (IL-6R) for downstream signaling [9]. The downstream signaling cascades of L-gp130 include JAK/STAT, PI3K/AKT, MEK/ERK, and Hippo/YAP (Fig. 1a, right panel), which are identical to those of wild type IL6ST signaling following binding of IL-6 ligand and IL-6R. To study the role of constitutively activated IL6ST signaling in vivo and to decipher the respective downstream signaling axis involved in PCa, the *L-gp130* transgene composed of a synthetic CMV-Actin-Globin composite (CAG) promotor mediating expression of *L-gp130* and *Zoanthus sp.* green fluorescent protein (ZSGreen) was integrated into the ROSA26 locus, which can be transcriptionally activated by Cre-mediated removal of the Westphal stop sequence [3]. We introduced this construct into a conditional mouse model with prostate epithelium-specific Cre expression with sexual maturity using Probasin (PB)-Cre4 mice [21, 23]. This approach generated mice with prostate epithelium-specific constitutively active L-gp130 alleles (*L-gp130*$^{peKI/KI}$; pe: prostate epithelium; KI: knock in). These *L-gp130*$^{peKI/KI}$ mice were then crossed with mice in which *Pten* deletion occurs in the prostate epithelium upon PB-Cre4 expression, leading to the development of PCa (*Pten*$^{pe\Delta/\Delta}$; Δ: knock out) [20]. The crossbreed resulted in PCa mice with additional prostate epithelium-specific constitutively activated IL6ST signaling (*Pten*$^{pe\Delta/\Delta}$;*L-gp130*$^{peKI/KI}$) (Fig. 1b).

Deletion of *Pten* and insertion of *L-gp130* were confirmed after the onset of puberty by Polymerase Chain Reaction (PCR) (Supplementary Fig. 1a, Additional File 5). In addition, prostate epithelium-specific deletion of *Pten* was assessed by IHC analysis of phospho-AKT (p-AKT) levels, as loss of PTEN leads to phosphorylation of AKT [14]. *Pten*$^{pe\Delta/\Delta}$ and *Pten*$^{pe\Delta/\Delta}$;*L-gp130*$^{peKI/KI}$ showed elevated p-AKT expression compared to wild type and *L-gp130*$^{peKI/KI}$ prostate samples (Fig. 1c, upper panel). Further confirmation of prostate-specific deletion of *Pten* was obtained by Western blot analysis and quantification of p-AKT levels. *Pten*$^{pe\Delta/\Delta}$ and *Pten*$^{pe\Delta/\Delta}$;*L-gp130*$^{peKI/KI}$ showed significantly increased p-AKT expression compared to wild type and *L-gp130*$^{peKI/KI}$ prostate samples, whereas total-AKT (t-AKT) expression was not affected between the different genotypes (Supplementary Fig. 1b-c, Additional File 5). To confirm the functional expression of the *L-gp130* construct, we examined ZSGreen expression via IF. We found ZSGreen expression in *L-gp130*$^{peKI/KI}$ and *Pten*$^{pe\Delta/\Delta}$;*L-gp130*$^{peKI/KI}$ but not in wild type and *Pten*$^{pe\Delta/\Delta}$ prostates (Fig. 1c, lower panel). Of note, endogenous wild type *Il6st* mRNA levels were not changed by *L-gp130* expression in the prostate (Supplementary Fig. 1d, Additional File 5). This is in line with previous findings revealing no impact on endogenous IL6ST expression by the introduction of the L-gp130 construct [3]. Overall, we generated a mouse model allowing us to examine the consequences of cell-autonomous, prostate epithelial cell-specific IL6ST signaling.

Constitutively active IL6ST signaling reduces *Pten*-deficient tumor growth in vivo

We next examined the impact of constitutively active IL6ST signaling in 19-week old mice and found that prostates of wild type and *L-gp130*$^{peKI/KI}$ mice were macroscopically indistinguishable. As expected, *Pten*$^{pe\Delta/\Delta}$ mice developed grossly visible PCa (Fig. 1d). Intriguingly, mice with concomitant activation of IL6ST signaling (*Pten*$^{pe\Delta/\Delta}$;*L-gp130*$^{peKI/KI}$) developed smaller prostate tumors compared to *Pten*-deficient mice, resulting in a significantly reduced prostate weight of *Pten*$^{pe\Delta/\Delta}$;*L-gp130*$^{peKI/KI}$ compared to *Pten*$^{pe\Delta/\Delta}$ mice (Fig. 1d-e).

Assessment of H&E-stained murine prostates (Fig. 1f) revealed no pathological features in wild type and *L-gp130*$^{peKI/KI}$ mice, except for one *L-gp130*$^{peKI/KI}$ animal (accounting for 11.1% of analyzed mice) (Fig. 1g). This animal exhibited prostatic intraepithelial neoplasia (PIN), a precursor for PCa. The vast majority (72.7%) of the *Pten*$^{pe\Delta/\Delta}$ mice showed PCa [34], whereas only 22.2% of *Pten*$^{pe\Delta/\Delta}$;*L-gp130*$^{peKI/KI}$ mice developed PCa. Instead, 77.8% exhibited only PIN, displaying a less aggressive morphology compared to *Pten*$^{pe\Delta/\Delta}$ mice. These findings support a tumor-suppressive role of IL6ST signaling in PCa in vivo.

L-gp130 expression in prostate epithelial cells enriches STAT3 target gene expression

To unravel molecular gene expression patterns associated with the observed phenotypes and to elucidate which of the possible downstream signaling axes is activated upon *L-gp130* insertion, we performed RNA-Seq analysis of prostate tissue from wild type, *L-gp130*$^{peKI/KI}$, *Pten*$^{pe\Delta/\Delta}$ and *Pten*$^{pe\Delta/\Delta}$;*L-gp130*$^{peKI/KI}$ mice. As our mouse model allows prostate epithelium-specific modulation and to specifically isolate these prostate epithelial cells, we sorted cells obtained from prostate tissue by magnetic

bead-based cell sorting for EpCAM, a marker for epithelial cells that is expressed uniformly across all four genotypes (Fig. 2a). This prostate epithelial fraction was then subjected to RNA-Seq as previously described [22] (Fig. 2b). Clustering of the samples by 3D-principal component analysis based on gene expression revealed that individual replicates clustered within the genotypes and confirmed different transcription profiles (Supplementary Fig. 2a, Additional File 5). Differential gene expression analysis of *Pten*$^{peΔ/Δ}$ and *Pten*$^{peΔ/Δ}$;*L-gp130*$^{peKI/KI}$ prostate epithelial cells showed significant upregulation of 807 and downregulation of 475 genes in *Pten*$^{peΔ/Δ}$;*L-gp130*$^{peKI/KI}$ prostates (Fig. 2c). Notably, we detected nearly twice as many upregulated genes as downregulated genes, which supports the idea that constitutively active IL6ST serves as a central receptor of signal transduction and activator of transcription. There was also a considerable, albeit smaller number of 470 genes that were significantly upregulated when comparing *L-gp130*$^{peKI/KI}$ and wild type prostate epithelial cells, as well as 335 downregulated genes (Supplementary Fig. 2b, Additional File 5). Fast pre-ranked gene set enrichment analysis (fGSEA) of the "Prostate cancer" gene set from the Kyoto Encyclopedia of Genes and Genomes (KEGG) collection from the Molecular signature database (MSigDB) [35, 36] showed a significant downregulation of analyzed genes in *Pten*$^{peΔ/Δ}$;*L-gp130*$^{peKI/KI}$ compared to *Pten*$^{peΔ/Δ}$ samples (Fig. 2d), which supports our mouse data showing smaller tumors in *Pten*$^{peΔ/Δ}$;*L-gp130*$^{peKI/KI}$ mice.

To determine which downstream signaling cascade is activated by L-gp130 in PCa, we performed fGSEA of *Pten*$^{peΔ/Δ}$;*L-gp130*$^{peKI/KI}$ compared to *Pten*$^{peΔ/Δ}$ samples using the REACTOME gene set collection derived from MSigDB. We detected no apparent change in the regulation of PI3K/AKT, RAS/RAF/ERK/MAPK or Hippo/YAP signaling cascades (Supplementary Fig. 2c, Additional File 5). Interestingly, we found significantly upregulated STAT3 target genes by analyzing three independent, previously described sets of STAT3 target genes [37–39]. These results imply that *L-gp130* expression correlated with STAT3 activity, which in turn acts as a transcription factor in PCa (Fig. 2e). In accordance, Western blot analysis also showed activation of STAT3, reflected in increased phosphoY705-STAT3 (pY-STAT3) levels and unaltered total-STAT3 (t-STAT3) levels in *Pten*$^{peΔ/Δ}$;*L-gp130*$^{peKI/KI}$ compared to *Pten*$^{peΔ/Δ}$ prostates (Fig. 2f-g). This finding was further confirmed using IHC, which showed a nearly 50% increase in pY-Stat3 positive cells in *Pten*$^{peΔ/Δ}$;*L-gp130*$^{peKI/KI}$ compared to *Pten*$^{peΔ/Δ}$ samples, while t-STAT3 levels assessed semi-quantitatively were constant in both genotypes (Fig. 2h-j). This increase in pY-STAT3^{+} epithelial cells is on top of the already nearly 60% pY-STAT3^{+} epithelial cells seen in *Pten*$^{peΔ/Δ}$ samples. In addition to the classical activation of STAT3 via phosphorylation of Y705 [40], transcriptional activation can be regulated by phosphorylation at Ser727 [41]. PhosphoS727-STAT3 (pS727-STAT3) levels were significantly upregulated in *Pten*$^{peΔ/Δ}$;*L-gp130*$^{peKI/KI}$ compared to *Pten*$^{peΔ/Δ}$ prostates (Supplementary Fig. 2d-f, Additional File 5). In line, we observed an upregulation of STAT3 target genes (Supplementary Fig. 2g, Additional File 5) and of pY-STAT3 abundance (Supplementary Fig. 2h-l, Additional File 5) when comparing *L-gp130*$^{peKI/KI}$ and wild type prostate epithelial cells. Of note, in the stromal cells of mice with *L-gp130* insertion in the prostate epithelium (*L-gp130*$^{peKI/KI}$ and *Pten*$^{peΔ/Δ}$;*L-gp130*$^{peKI/KI}$ mice), we detected no increase in pY-STAT3 and

(See figure on next page.)

Fig. 2 L-gp130 leads to activation of the STAT3 transcription factor and STAT3 target gene expression. **a** Representative immunohistochemistry (IHC) pictures of mouse prostates stained for the epithelial marker EpCAM. Scale bar: 40 µm **b** RNA-Seq workflow showing processing and magnetic bead-based enrichment of EpCAM-positive (EpCAM^{+}) mouse prostate tissue. Prostates were dissected and enzymatically and mechanically dissociated to generate single cell suspensions. Cells were labeled with biotinylated anti-EpCAM antibody and enriched from the bulk population using streptavidin-coated magnetic beads. EpCAM^{+} cells were subjected to RNA-Seq analysis. **c** Heatmap and number of differentially expressed genes (log2norm) based on adj. p-value ≤ 0.05 and fold change ≥ 2 cut-off values comparing *Pten*$^{peΔ/Δ}$ and *Pten*$^{peΔ/Δ}$;*L-gp130*$^{peKI/KI}$ prostate epithelial cells (n ≥ 5). blue: downregulated, red: upregulated. **d** Fast pre-ranked gene set enrichment analysis (fGSEA) of the KEGG gene set "Prostate cancer" with genes regulated in *Pten*$^{peΔ/Δ}$;*L-gp130*$^{peKI/KI}$ compared to *Pten*$^{peΔ/Δ}$ prostate epithelial cells. Genes sorted based on their Wald statistics are represented as vertical lines on the x-axis. NES: normalized enrichment score. **e** fGSEA of three previously published STAT3 target signatures ("STAT3 targets (Swoboda)", "STAT3 targets (Azare)", "STAT3 targets (Carpenter)") with genes regulated in *Pten*$^{peΔ/Δ}$;*L-gp130*$^{peKI/KI}$ compared to *Pten*$^{peΔ/Δ}$ prostate epithelial cells. Genes sorted based on their Wald statistics are represented as vertical lines on the x-axis. NES: normalized enrichment score. **f** Western Blot analysis of prostate protein lysates for phosphoTyrosine705-STAT3 (pY-STAT3) and total-STAT3 (t-STAT3) expression in *Pten*$^{peΔ/Δ}$ and *Pten*$^{peΔ/Δ}$;*L-gp130*$^{peKI/KI}$ mice ($n = 5$). β-ACTIN (β-ACT) served as loading control. **g** Quantification of pY-STAT3 protein levels relative to t-STAT3 protein levels shown in f). **h** Representative pictures of IHC staining of pY-STAT3 and t-STAT3 expression in prostate sections of *Pten*$^{peΔ/Δ}$ and *Pten*$^{peΔ/Δ}$;*L-gp130*$^{peKI/KI}$ mice. Scale bar: 40 µm. **i-j** Quantitative analysis of pY-STAT3 (i) and semi-quantitative analysis of t-STAT3 (j) IHC stainings shown in h) ($n = 7$). **g**,**i-j** Individual biological replicates are shown (g,i). Data are plotted as the means ± SD and p-values were determined by unpaired two-tailed Student's t-tests (g,i) or Mann-Whitney test (j)

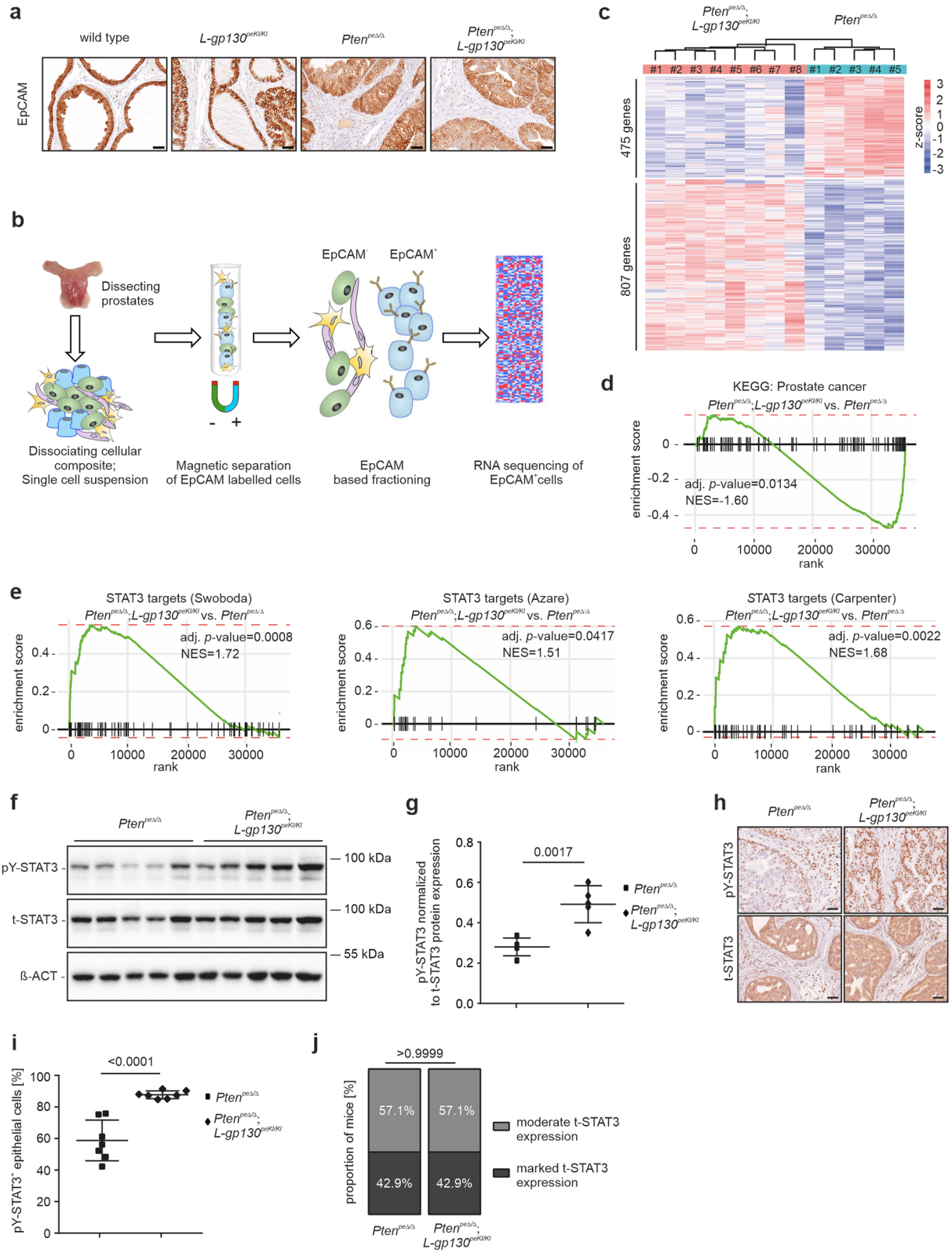

Fig. 2 (See legend on previous page.)

pS727-STAT3 levels compared to wild type and *Pten*$^{peΔ/Δ}$ mice, respectively (Supplementary Fig. 2m-n, Additional File 5). This underscores the prostate-epithelium specificity of our mouse model. Taken together, L-gp130 expression in prostate epithelial cells activates STAT3 signaling, as evidenced by significantly upregulated STAT3 target genes and increased pY-STAT3 and pS727-STAT3 levels.

IL6ST expression correlates with prolonged survival and STAT3 expression in PCa patients

Based on our mouse data, we hypothesized that high IL6ST expression in PCa patients would correlate with favorable clinical outcomes. To investigate the relationship between *IL6ST* mRNA expression levels and PCa, we examined the TCGA-PRAD cohort [28] comprising primary PCa patients and found a significant decrease in *IL6ST* mRNA expression in prostate tumor tissue compared to adjacent healthy tissue (Fig. 3a). We divided patients into *IL6ST* high and low expression groups using the maximally selected rank statistics method, which identifies the cutpoint with the most significant relation with disease-free survival. Stratifying patients based on their *IL6ST* mRNA demonstrated that high *IL6ST* expression is linked to a greater probability of disease-free survival compared to low *IL6ST* expression (Fig. 3b). In the TCGA-PRAD cohort, 7.2% of patients with prostate adenocarcinoma have alterations in the *IL6ST* gene, with 6.3% accounting for deep deletions and 0.9% for missense mutations of unknown significance (Fig. 3c). We therefore hypothesized that mutations leading to altered *IL6ST* expression could impact the initiation and/or progression of PCa. To test the validity of our findings, we analyzed four additional data sets from the Oncomine platform [42]. The results support a significant decrease in *IL6ST* mRNA expression in PCa compared to normal prostate glands, highlighting the potential impact of IL6ST alterations on PCa (Fig. 3d). We also observed a significant reduction in *IL6ST* expression relative to the primary PCa site during PCa progression in recurrent and advanced PCa and metastasis (Supplementary Fig. 3a, Additional File 5). Using the SurvExpress Analysis webtool [43], we next examined the MSKCC Prostate GSE21032 data set by Taylor et al. [44] in terms of survival, as it provides not only data on primary but also metastatic PCa. We assessed risk groups by a median split of samples based on their prognostic index and observed high expression of *IL6ST* in low-risk PCa patients and vice versa (Supplementary Fig. 3b, Additional File 5). In support of our previous findings from the TCGA-PRAD cohort, correlating biochemical recurrence-free survival time with *IL6ST* mRNA expression levels, we detected a significantly higher probability of biochemical recurrence-free survival associated with high as compared to low *IL6ST* levels (Supplementary Fig. 3c, Additional File 5). To further validate our findings in an independent dataset, we analyzed the SMD GSE40727 [45] cohort using the SurvExpress Analysis web tool. Survival analysis of patients expressing high and low levels of *IL6ST*, grouped according to the optimal risk split, showed a tendency for better biochemical recurrence-free survival probability in the *IL6ST*^{high} group compared to the *IL6ST*^{low} group (Supplementary Fig. 3d-e, Additional File 5). These findings corroborate a tumor suppressive role of *IL6ST* expression in PCa. Interestingly, *IL6ST* mRNA expression positively correlated with *STAT3* expression in PCa patients in both the TCGA-PRAD cohort and Taylor data set (MSKCC Prostate GSE21032), providing further evidence of the interconnected signaling between IL6ST and STAT3 in PCa (Fig. 3e and Supplementary Fig. 3f, Additional File 5). To examine the IL6ST/STAT3 signaling activation in the TCGA-PRAD data set, we correlated *IL6ST* (Supplementary Fig. 3g, Additional File 5) and *STAT3* (Supplementary Fig. 3h, Additional File 5) mRNA expression levels with three STAT3 target signatures assessed by single sample gene set variation analysis (ssGSVA). All three STAT3 target gene sets were positively correlated to *IL6ST* and *STAT3* mRNA expression levels indicating a tight association of high *IL6ST* and *STAT3* expression and active STAT3 signaling. Together, these human patient data suggest that *IL6ST* expression could serve as a useful read-out to stratify PCa cases into low- and high-risk groups.

L-gp130 promotes STAT3/p19^{ARF}/p53-induced senescence upon *Pten*-loss

To further understand the molecular mechanisms underlying the observed reduction in tumor size in mice expressing constitutively active *Il6st* in the prostate epithelium, we investigated changes in gene expression. Performing fGSEA using the HALLMARK gene set collection from MSigDB, we identified significantly deregulated gene sets that rely on L-gp130 expression in prostate tumorigenesis. Upon *L-gp130* insertion, the "IL-6/JAK/STAT3 signaling" gene set was upregulated in *L-gp130*$^{peKI/KI}$ and *Pten*$^{peΔ/Δ}$;*L-gp130*$^{peKI/KI}$ mice, compared to wild type and *Pten*$^{peΔ/Δ}$ mice, respectively (Fig. 4a and Supplementary Fig. 4a, Additional File 5). This is noteworthy as IL-6 activates the Janus kinase (JAK) and subsequently STAT3 by binding to the IL6ST receptor [9], and therefore upregulated "IL-6/JAK/STAT3 signaling" aligns with our previous results on the induction of the STAT3 signaling cascade. From all HALLMARK gene sets, we found 32 being significantly deregulated when comparing *Pten*$^{peΔ/Δ}$;*L-gp130*$^{peKI/KI}$ and *Pten*$^{peΔ/Δ}$ samples. Among these gene

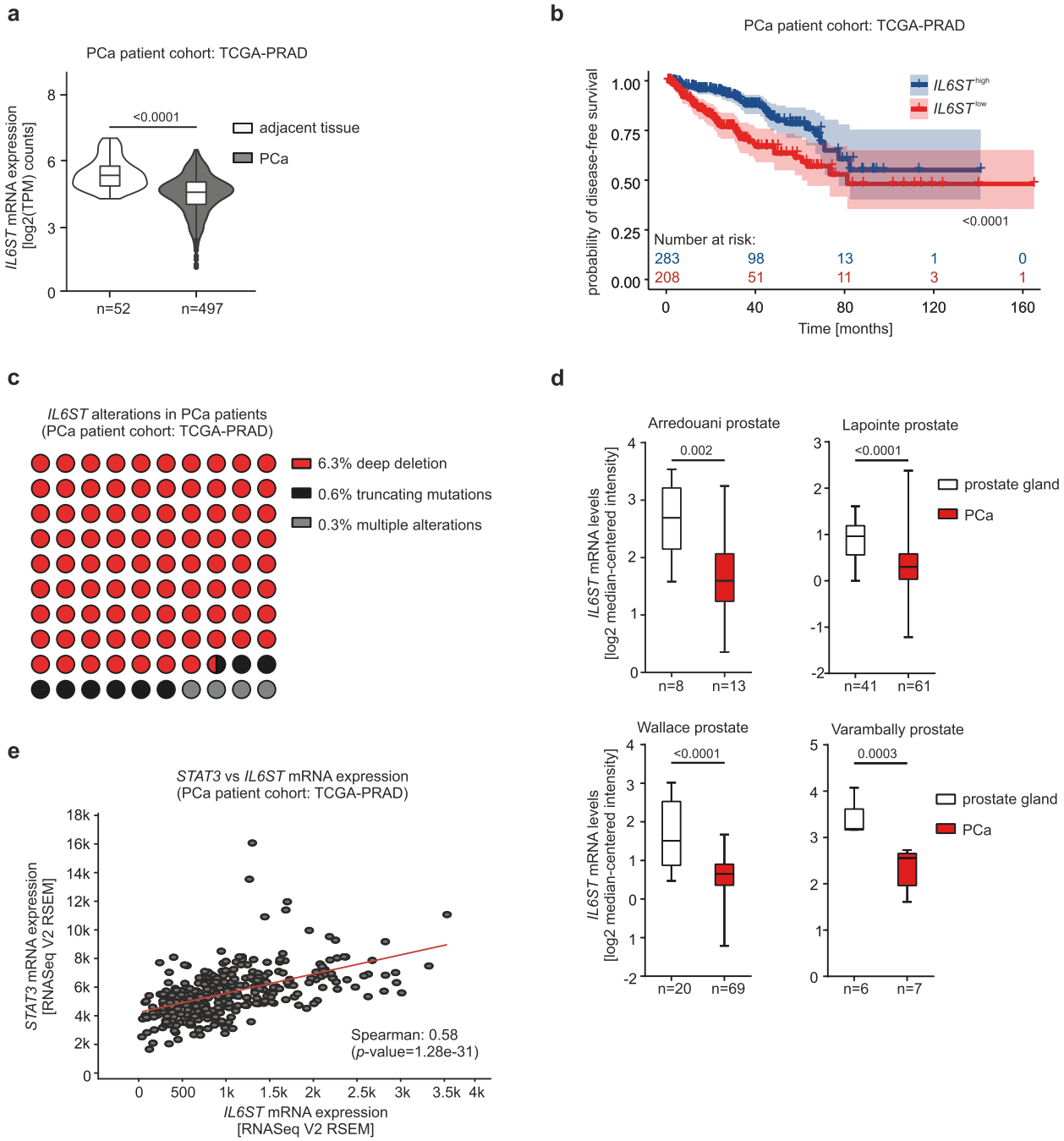

Fig. 3 High *IL6ST* expression is significantly associated with low-risk groups and better recurrence-free survival in human PCa. **a** *IL6ST* gene expression in adjacent ($n=52$) and PCa ($n=497$) tissue in TCGA-PRAD data set. Statistical analysis of the two risk groups was determined by using the Mann–Whitney test. **b** Kaplan–Meier plot showing time of disease-free survival in months for $IL6ST^{low}$ and $IL6ST^{high}$ risk groups of the TCGA-PRAD data set. Groups were assessed based on the maximally selected rank statistics. blue: high *IL6ST* expressing group, red: low *IL6ST* expressing group. The blue and red numbers above horizontal axis represent the number of patients. **c** Proportion of *IL6ST* alterations in the TCGA-PRAD data set. Mutation types: deep deletion ($n=21$; red), truncating mutations ($n=2$; black) and multiple alterations ($n=1$; grey). One patient has simultaneous mutations. The data originate from cBioPortal. **d** *IL6ST* mRNA expression levels of four different data sets of PCa patient samples compared to healthy prostate sample control. Normalized data and statistical analyses were extracted from the Oncomine Platform. The respective prostate data set and n-numbers are indicated. Representation: boxes as interquartile range, horizontal line as the mean, whiskers as lower and upper limits. **e** Spearman-correlation analysis of *IL6ST* and *STAT3* expression in TCGA-PRAD data set using cBioPortal analysis tool

sets, the downregulated HALLMARK gene set "Androgen response" (Fig. 4a) points to less androgen receptor signaling in *Pten*$^{peΔ/Δ}$;*L-gp130*$^{peKI/KI}$ mice, which is in line with its crucial role in PCa development [46] and the observed reduction in cancer aggressiveness in our *Pten*$^{peΔ/Δ}$;*L-gp130*$^{peKI/KI}$ mice. The two HALLMARK gene sets showing the most pronounced downregulation were "Oxidative phosphorylation" and "Fatty acid metabolism". This observation is noteworthy as we have previously demonstrated an inverse association between the regulation of oxidative phosphorylation and the TCA cycle with STAT3 expression [47, 48]. This downregulation is also seen in the corresponding KEGG and Biological Processes from Gene Ontology pathways (GO-BP) gene sets (Supplementary Fig. 4b, Additional File 5). Given that the downregulation of these pathways has previously been shown to rely on STAT3 signaling, it underscores the importance of active STAT3 signaling in the context of this study. Surprisingly, the two most prominent upregulated gene sets are the proliferation-associated "MYC targets V1" and "MYC targets V2" (Fig. 4a). We also observed an upregulation of MYC target genes in the comparison of *L-gp130*$^{peKI/KI}$ and wild type (Supplementary Fig. 4a, Additional File 5). As *MYC* gene expression is regulated by IL6ST/STAT3 [49], this might contribute to the observed upregulation of MYC target genes in both comparisons (*Pten*$^{peΔ/Δ}$;*L-gp130*$^{peKI/KI}$ versus *Pten*$^{peΔ/Δ}$ and *L-gp130*$^{peKI/KI}$ versus wild type). Additionally, the cell cycle-related gene sets "E2F targets" and "G2M checkpoint" were significantly upregulated. Considering the reported potential of the IL-6/STAT3 axis to drive rather than inhibit tumor cell proliferation [50], we investigated proliferation. We did not observe a significant difference in Ki67 assessed by IHC staining (Fig. 4b-c). Another gene set that was observed to be significantly upregulated is the "P53 pathway", which is known to mediate oncogene-induced senescence in prostate tumorigenesis [51, 52] and in the *Pten*-deficient PCa context [8]. Therefore we hypothesized that the induction of senescence in *Pten*$^{peΔ/Δ}$;*L-gp130*$^{peKI/KI}$ compared to *Pten*$^{peΔ/Δ}$ mice causes the smaller tumors observed in *Pten*$^{peΔ/Δ}$;*L-gp130*$^{peKI/KI}$ mice. Senescence is often accompanied by the upregulation of promyelocytic leukemia protein (PML) [53]. Indeed, we observed increased numbers of PML nuclear bodies in our *Pten*$^{peΔ/Δ}$;*L-gp130*$^{peKI/KI}$ mice (Fig. 4d-e). An additional defining characteristic of senescent cells is the release of inflammatory cytokines and signaling molecules referred to as SASP [17]. To investigate the alteration of SASP-related genes in *Pten*$^{peΔ/Δ}$;*L-gp130*$^{peKI/KI}$ prostate epithelial cells, we performed fGSEA using the "Core SASP of Pten-loss induced cellular senescence (PICS)" [54] gene set, previously described to be induced upon PICS, and found it to be significantly upregulated in *Pten*$^{peΔ/Δ}$;*L-gp130*$^{peKI/KI}$ mice compared to *Pten*$^{peΔ/Δ}$ mice (Supplementary Fig. 4c, Additional File 5).

Upon closer examination of the molecular players involved in senescence induction, we found that the p19^{ARF}/p53-dependent pathway was activated. We observed significantly enhanced expression of *Cdkn2a* mRNA, which encodes both *p16*^{INK4A} and *p19*^{ARF} (Fig. 4f) [55]. Using *p19*^{ARF} specific primers revealed a significant upregulation of this previously described STAT3 target gene [8] (Fig. 4g). We observed a significant increase in p53 protein abundance (Fig. 4h-i). In line with this, we also noted that gene sets representing transcriptional p53 activity were significantly upregulated in our fGSEA of GO-BP gene sets derived from MSigDB (Supplementary Fig. 4d, Additional File 5). Based on our data, we thus propose a model of IL6ST signaling-induced senescence in PCa, in which STAT3, activated by L-gp130, upregulates *p19*^{ARF} mRNA expression, followed by increased p53 expression and induction of senescence as seen by elevated PML expression (Fig. 4j).

(See figure on next page.)

Fig. 4 Expression of L-gp130 induces p19^{ARF}-p53-driven senescence in *Pten*-deficient PCa. **a** Fast pre-ranked gene set enrichment analysis (fGSEA) of significantly enriched HALLMARK gene sets with genes regulated in *Pten*$^{peΔ/Δ}$;*L-gp130*$^{peKI/KI}$ compared to *Pten*$^{peΔ/Δ}$ prostate epithelial cells. Dotted line: adj. p-value (-log10(0.05)), blue: downregulated, red: upregulated; **b** Representative pictures of immunohistochemistry (IHC) staining of mouse prostates from the indicated genotypes stained for the proliferation marker Ki67. Scale bar: 40 µm. **c** Semi-quantitative analysis of Ki67^{+} prostate epithelial cells in the indicated genotypes ($n = 7$) shown in b). **d** Representative pictures of IHC staining of PML of *Pten*$^{peΔ/Δ}$ and *Pten*$^{peΔ/Δ}$;*L-gp130*$^{peKI/KI}$ prostates. Scale bar: 40 µm. **e** Quantification of PML nuclear bodies per high power field (HPF) shown in d) ($n \geq 5$). **f** *Cdkn2a* mRNA expression levels based on normalized counts from RNA-Seq analysis of *Pten*$^{peΔ/Δ}$ and *Pten*$^{peΔ/Δ}$;*L-gp130*$^{peKI/KI}$ prostates ($n \geq 5$). **g** qRT-PCR mRNA expression analysis of *p19*^{ARF} in mouse prostate tissue of *Pten*$^{peΔ/Δ}$ and *Pten*$^{peΔ/Δ}$;*L-gp130*$^{peKI/KI}$ mice ($n \geq 5$). Signals are relative to the geometric mean of housekeeping genes. **h** Western Blot analysis of prostate protein lysates of *Pten*$^{peΔ/Δ}$ and *Pten*$^{peΔ/Δ}$;*L-gp130*$^{peKI/K}$ mice ($n = 5$) for p53 expression. β-ACTIN (β-ACT) served as loading control. **i** Quantification of p53 protein levels shown in h) normalized to loading control. **j** Proposed model of IL6ST signaling induced senescence. L-gp130 activated STAT3 binds to its binding sites in Cdkn2a promoter, followed by upregulation of p19^{ARF} and p53 expression promoting senescence in PCa. **c**,**e**–**g**,**i** Individual biological replicates are shown (e–g,i). Data are plotted as the means ± SD and p-values were determined by Mann–Whitney test (c,f), unpaired two-tailed Student's t-tests (e,g,i)

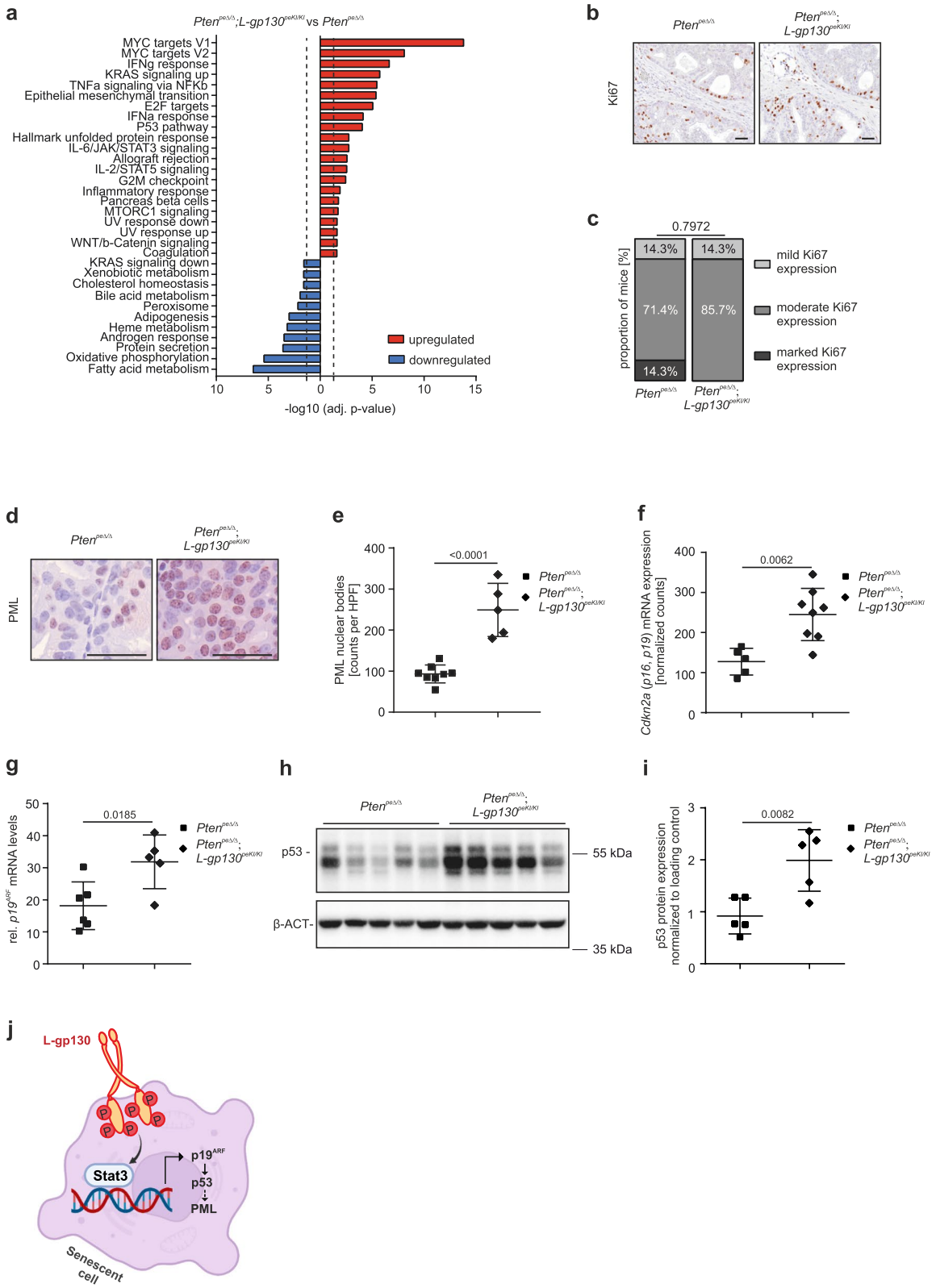

Fig. 4 (See legend on previous page.)

IL6ST signaling recruits anti-tumor infiltrating immune cells

Senescence is closely connected to the TME, known to be immune-cold in PCa [19]. Consequently, we focused our examination on the impact of constitutively active IL6ST on the TME. Indeed, upon analysis of H&E stained prostate sections we detected high-grade immune cell infiltration in 66.7% of *Pten*$^{peΔ/Δ}$;*L-gp130*$^{peKI/KI}$ mice compared to 36.4% of *Pten*$^{peΔ/Δ}$ mice (Fig. 5a). Only few immune cells were seen in wild type and *L-gp130*$^{peKI/KI}$ prostates (Supplementary Fig. 5a, Additional File 5). IF analysis allowed us to examine the infiltrating immune cell subtypes and their distribution and revealed a significantly higher number of CD45$^+$ cells in *Pten*$^{peΔ/Δ}$;*L-gp130*$^{peKI/KI}$ mice compared to *Pten*$^{peΔ/Δ}$ mice and the occurrence of minimal CD45$^+$ cells in wild type and *L-gp130*$^{peKI/KI}$ mice (Fig. 5b-c and Supplementary Fig. 5b-c, Additional File 5).

A more detailed characterization showed that L-gp130 expression did not affect B-cell (CD79b) involvement in immune cell infiltration (Supplementary Fig. 5d-e, Additional File 5). Importantly, CD3$^+$ cells were significantly increased in the prostate epithelium of *Pten*$^{peΔ/Δ}$;*L-gp130*$^{peKI/KI}$ mice (Supplementary Fig. 5f-g, Additional File 5), whereas, in the adjacent stroma, the CD3$^+$ cell levels did not exhibit a significant difference compared to *Pten*$^{peΔ/Δ}$ mice (Supplementary Fig. 5h, Additional File 5). Notably, a substantial proportion of these cells were CD3$^+$;CD8$^+$ positive (Fig. 5d and Supplementary Fig. 5i-j, Additional File 5), which are considered major drivers of anti-tumor immunity [56]. We also noted a significant difference in the ability of CD3$^+$;CD8$^+$ cells to migrate into the epithelium between *Pten*$^{peΔ/Δ}$ and *Pten*$^{peΔ/Δ}$;*L-gp130*$^{peKI/KI}$ mice (Fig. 5e), whereas their proportion in the stroma was unaffected by L-gp130 expression (Supplementary Fig. 5k, Additional File 5). Concurrently, our findings indicated that CD3$^+$;CD4$^+$ T-cells did not play a significant role in anti-tumor infiltration in our mouse model (Supplementary Fig. 5l-n, Additional File 5).

Next, we examined neutrophils and macrophages to understand their potential contributions to the immune response within the prostate epithelium and the TME. IHC stainings for the neutrophil marker NimpR14 and macrophage marker F4/80 revealed a significant increase in the epithelial fraction of *Pten*$^{peΔ/Δ}$;*L-gp130*$^{peKI/KI}$ compared to *Pten*$^{peΔ/Δ}$ prostates (Fig. 5f-h), but no change in stroma or in the comparison of wild type and *L-gp130*$^{peKI/KI}$ mice (Supplementary Fig. 5o-t, Additional File 5), reflecting innate immune cell tumor infiltration upon constitutive IL6ST signaling activation in *Pten*$^{peΔ/Δ}$;*L-gp130*$^{peKI/KI}$ mice. To characterize and distinguish M1 and M2 macrophages, we performed flow cytometry using CD86 and MHC class II for M1, and CD206 for M2. Results indicated a proinflammatory and tumor-suppressive M1-like phenotype in *Pten*$^{peΔ/Δ}$;*L-gp130*$^{peKI/KI}$ prostates, evidenced by significantly downregulated CD206 expression and a tendency towards upregulated CD86 and MHC class II compared to *Pten*$^{peΔ/Δ}$ prostates (Fig. 5i-j). Interestingly, selected adaptive and innate immune system-related gene sets associated with chemotaxis, migration, regulation, and activation of immune cells were significantly upregulated when comparing *Pten*$^{peΔ/Δ}$;*L-gp130*$^{peKI/KI}$ with *Pten*$^{peΔ/Δ}$ samples (Supplementary Fig. 5u, Additional File 5), further substantiating the importance of infiltrating immune cells, specifically T-cells, neutrophils and macrophages, in our mouse model of PCa.

Given the importance of inflammatory cytokines in regulating the recruitment and activation of T-cells, neutrophils, and macrophages, we screened the significantly deregulated HALLMARK gene sets for related genes sets. Indeed, the gene set "Inflammatory response"

(See figure on next page.)

Fig. 5 Expression of L-gp130 in *Pten*$^{peΔ/Δ}$ mice increases infiltration of immune cells mediating anti-tumor defense. **a** Representative pictures of hematoxylin & eosin (H&E) stains (upper panel) showing immune infiltrate and quantification of histopathological analysis (lower panel) of prostate tissue from *Pten*$^{peΔ/Δ}$ ($n = 11$) and *Pten*$^{peΔ/Δ}$;*L-gp130*$^{peKI/KI}$ ($n = 9$) mice in regards of infiltration (low-grade (grey) and high-grade (red)). Scale bar: 60 µm. **b** Representative pictures of immunofluorescence (IF) staining of CD45 (red) and DAPI (blue) of mouse prostates with indicated genotypes. DAPI is used as a nuclear stain. Scale bar: 20 µm. **c** Quantification of CD45$^+$ cells of IF stainings shown in b) ($n = 5$). The percentage of positive cells relative to *Pten*$^{peΔ/Δ}$ was calculated. **d** Representative pictures of immunofluorescence (IF) staining of CD3 (yellow), CD8 (green) and DAPI (blue) of mouse prostates with indicated genotypes. DAPI is used as a nuclear stain. Scale bar: 20 µm. **e** Quantification of CD3$^+$;CD8$^+$ cells in the epithelium of IF stainings shown in d) ($n = 5$). The percentage of positive cells in the prostate epithelium relative to *Pten*$^{peΔ/Δ}$ was calculated. **f** Representative pictures of immunohistochemistry (IHC) staining of NimpR14 (higher panel) and F4/80 (lower panel) of mouse prostates with indicated genotypes. Scale bar: 40 µm. **g**-**h**) Quantification of NimpR14$^+$ (g) and F4/80$^+$ (h) cells in the prostate epithelium of IHC stainings shown in f) ($n \geq 6$). The percentage of positive cells in the prostate epithelium relative to *Pten*$^{peΔ/Δ}$ was calculated. **i**) Flow cytometry data showing mean fluorescence intensity (MFI) of F4/80$^+$;Cd11b$^+$ macrophages in *Pten*$^{peΔ/Δ}$ and *Pten*$^{peΔ/Δ}$;*L-gp130*$^{peKI/KI}$ prostate tissue ($n \geq 3$) for CD86, MHC class II, and CD206. **j** Representative flow cytomentry blots of data shown in i. **k** Representative pictures of IHC staining of CD3, NimpR14 and F4/80 (in presented order) of *Pten*$^{peΔ/Δ}$ and *Pten*$^{peΔ/Δ}$;Stat3$^{peΔ/Δ}$ prostates. Scale bar: 40 µm. **l** Semi-quantitative analysis of CD3, NimpR14 and F4/80 IHC stainings shown in k) ($n \geq 3$). **c, e, g-i, l** Individual biological replicates are shown (c,e,g-i). Data are plotted as the means ± SD and p-values were determined by unpaired two-tailed Student's t-tests (c,e,g-i) or Mann–Whitney test (l)

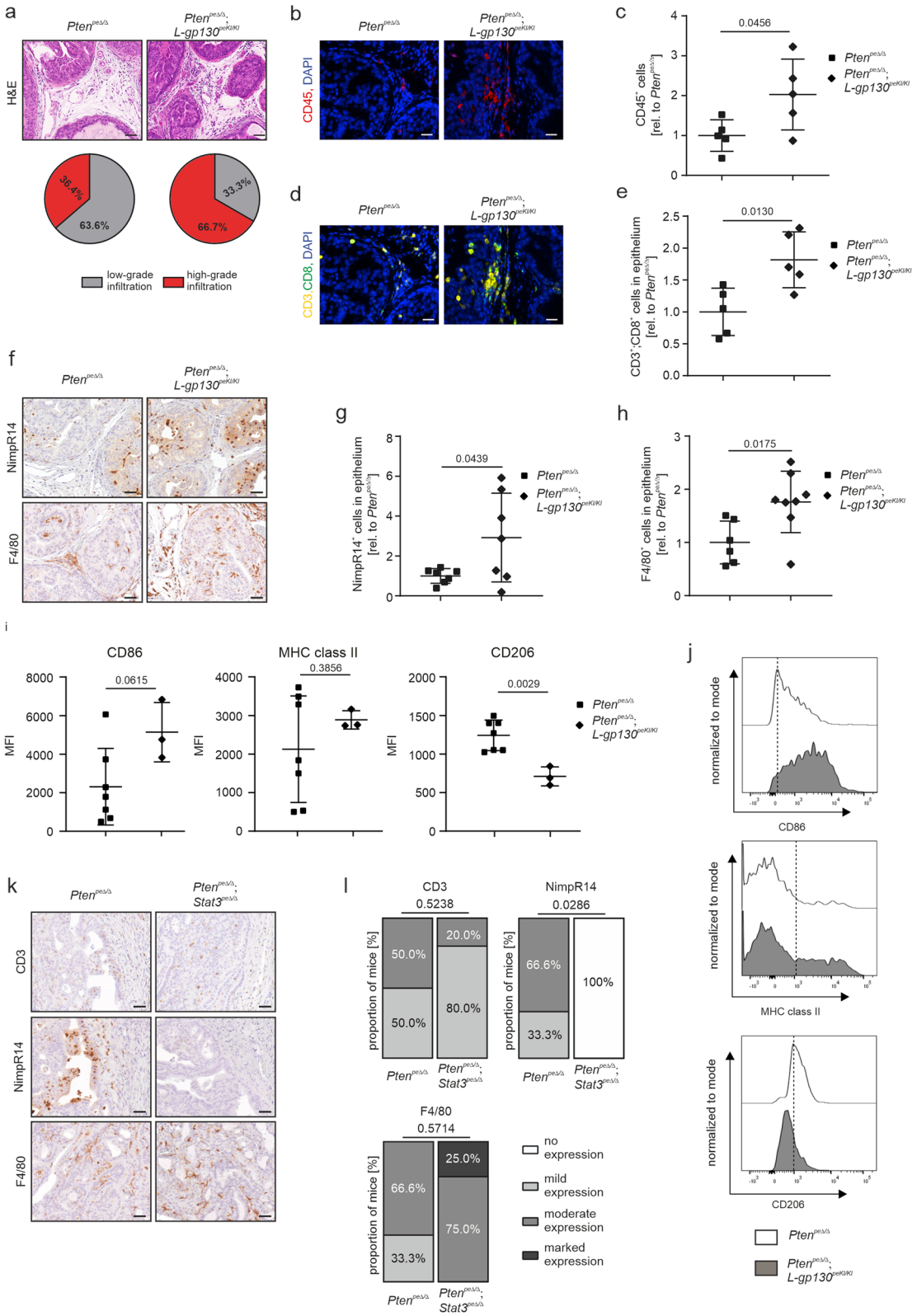

Fig. 5 (See legend on previous page.)

and signaling of the effector molecules IFNγ and TNFα, which are secreted by cytotoxic T-cells and affect tumor cells [57, 58], were significantly upregulated in our RNA-Seq data set (Fig. 4a). In order to delineate the cytokine profile more comprehensively, we analyzed serum samples obtained from the PCa mouse model. We specifically assessed the expression levels of various cytokines, chemokines, and receptors, including VEGF, CCL5, TNFα, IL-1α, IL-2R, IL-12p70, CXCL1, CXCL5, CXCL10, CD27, G-CSF. The multiplex immunobead assay analysis revealed a significant alteration in the cytokine profile, characterized by a significant upregulation of the expression of inflammatory cytokines in the serum of *Pten*$^{peΔ/Δ}$;*L-gp130*$^{peKI/KI}$ mice compared to the *Pten*$^{peΔ/Δ}$ group (Supplementary Fig. 5v, Additional File 5). Taken together, these findings provide evidence that constitutively active IL6ST signaling in prostate epithelial cells, possibly through modifying the chemokine/cytokine profile, promotes the recruitment of T-cells, neutrophils, and macrophages and reshapes the TME towards higher infiltration susceptibility.

To provide mechanistic evidence that these alterations depend on STAT3 signaling, we utilized a previously established PCa mouse model featuring *Pten*$^{peΔ/Δ}$ with an additional prostate epithelium-specific deletion of *Stat3* (*Pten*$^{peΔ/Δ}$;*Stat3*$^{peΔ/Δ}$). These mice exhibit rapid tumor proliferation, metastasis, and an early death, in contrast to the slow, localized tumor progression seen in *Pten*$^{peΔ/Δ}$ mice [8]. Interestingly, several immune response-related pathways are downregulated in *Pten*$^{peΔ/Δ}$;*Stat3*$^{peΔ/Δ}$ compared to *Pten*$^{peΔ/Δ}$ prostates [47]. Consistent with these findings and our data in *Pten*$^{peΔ/Δ}$;*L-gp130*$^{peKI/KI}$ mice, *Pten*$^{peΔ/Δ}$;*Stat3*$^{peΔ/Δ}$ prostates showed no increase in the infiltration of CD3^{+} T-cells and F4/80^{+} macrophages, and a significant decrease in NimpR14^{+} neutrophils compared to *Pten*$^{peΔ/Δ}$ mice (Fig. 5k-l) highlighting the importance of STAT3 in immune cell infiltration in *Pten*-deficient PCa mice with concomitant active IL6ST signaling.

IL6ST signaling in PCa patients promotes STAT3 activation, senescence upregulation, elevated immune scores, and T-cell mediated cytotoxicity

To address the human relevance of our findings concerning the involvement of senescence and anti-tumor immunity in the proposed tumor-suppressive role of IL6ST/STAT3 signaling, we refined our analysis of the TCGA-PRAD patient data set by distinguishing *IL6ST*^{high} and *IL6ST*^{low} groups based on *IL6ST* mRNA expression levels (Fig. 3b). The fGSEA of HALLMARK gene sets revealed that "IL-6/JAK/STAT3 signaling" was upregulated in *IL6ST*^{high} compared with *IL6ST*^{low} patients (Fig. 6a), as evidenced by increased STAT3 target genes expression (Supplementary Fig. 6a, Additional File 5). The observed downregulation of "Oxidative phosphorylation" is in accordance with the inverse association with STAT3 [47] and the corresponding KEGG gene set (Supplementary Fig. 6b, Additional File 5).

As we depicted alterations in senescence and cell cycle regulators in our in vivo mouse model, we performed fGSEA excluding any patients with *TP53* mutations (Supplementary Table 4, Additional File 1). Analysis of senescence-related gene sets (previously published "Core SASP of PICS (Guccini)" [54] and "Fridman senescence up" taken from curated gene sets, class chemical and genetic perturbations (CGP)) revealed their significant upregulation in *IL6ST*^{high} PCa patients (Fig. 6b), providing a possible explanation for their improved survival (Fig. 3b). These patients also exhibited downregulation of cell cycle gene sets ("REACTOME: Cell cycle" and "REACTOME: G1/S transition") and upregulation of p53 signaling ("WikiPathways (WP): p53 transcriptional gene network") (Fig. 6c).

Using ESTIMATE (Estimation of STromal and Immune cells in MAlignant Tumor tissues using Expression data), a tool for predicting tumor purity, and the presence of infiltrating stromal/immune cells in tumor tissues based on gene expression data [32], we confirmed that the majority of PCa patients can be considered immune-cold

(See figure on next page.)

Fig. 6 IL6ST signaling in PCa patients actives STAT3 signaling and upregulates senescence, immune score and cytotoxicity. **a** Fast pre-ranked gene set enrichment analysis (fGSEA) of significantly enriched HALLMARK gene sets with genes regulated in *IL6ST*^{high} compared to *IL6ST*^{low} expressing patients from the TCGA-PRAD data set. Dotted line: adj. p-value (-log10(0.05)), blue: downregulated, red: upregulated; **b** fGSEA of the previously described core SASP gene signature upon PICS "Core SASP of PICS (Guccini)" (upper panel) and the curated gene set, class chemical and genetic perturbations (CGP) "CGP: Fridman senescence up" (lower panel) with genes regulated in *IL6ST*^{high} compared to *IL6ST*^{low} expressing patients from the TCGA-PRAD data set. Genes sorted based on their Wald statistics are represented as vertical lines on the x-axis. NES: normalized enrichment score. **c** fGSEA of WikiPathways (WP) gene sets "REACTOME: Cell cycle", "REACTOME: G1/S transition" and "WP: p53 transcriptional gene network" with genes regulated in *IL6ST*^{high} compared to *IL6ST*^{low} expressing patients from the TCGA-PRAD data set. Genes sorted based on their Wald statistics are represented as vertical lines on the x-axis. NES: normalized enrichment score. **d** Immune score from the ESTIMATE method for *IL6ST*^{low} (red, $n = 208$) and *IL6ST*^{high} (blue, $n = 283$) patients from the TCGA-PRAD data set, compared with Mann–Whitney test. **e** fGSEA of the top 20 T-cell-, neutrophil-, and macrophage-associated Biological Processes from Gene Ontology pathways (GO-BP) gene sets with genes significantly regulated in *IL6ST*^{high} compared to *IL6ST*^{low} expressing patients from the TCGA-PRAD data set. Dotted line: adj. p-value (-log10(0.05)), red: upregulated;

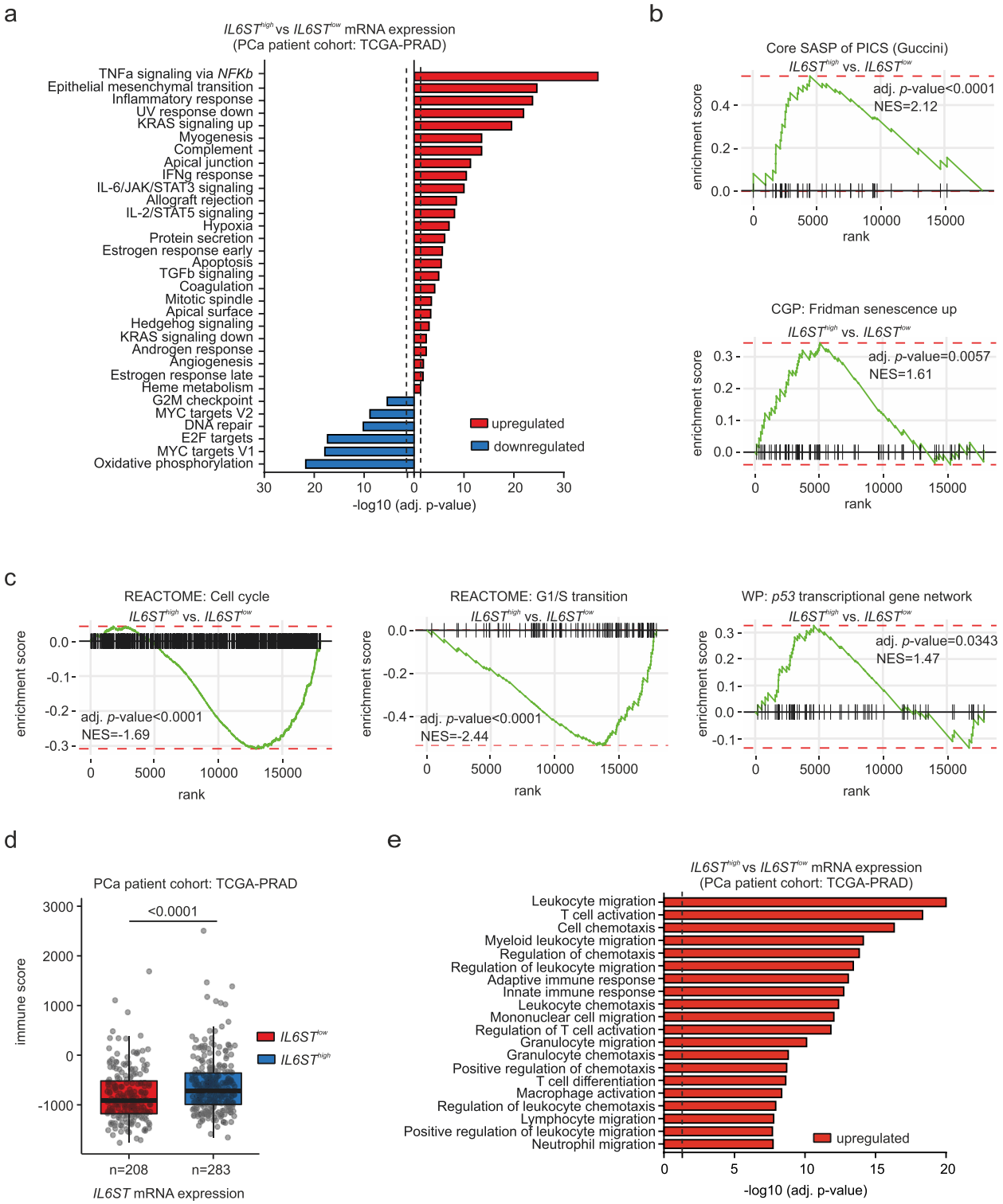

Fig. 6 (See legend on previous page.)

due to their low immune scores (Supplementary Fig. 6c, Additional File 5). Notably, higher immune scores have been associated with longer survival rates in PCa patients [59]. In our patient cohort, *IL6ST*^{high} patients showed significantly higher immune scores compared to *IL6ST*-^{low} patients (Fig. 6d), correlating with the upregulation

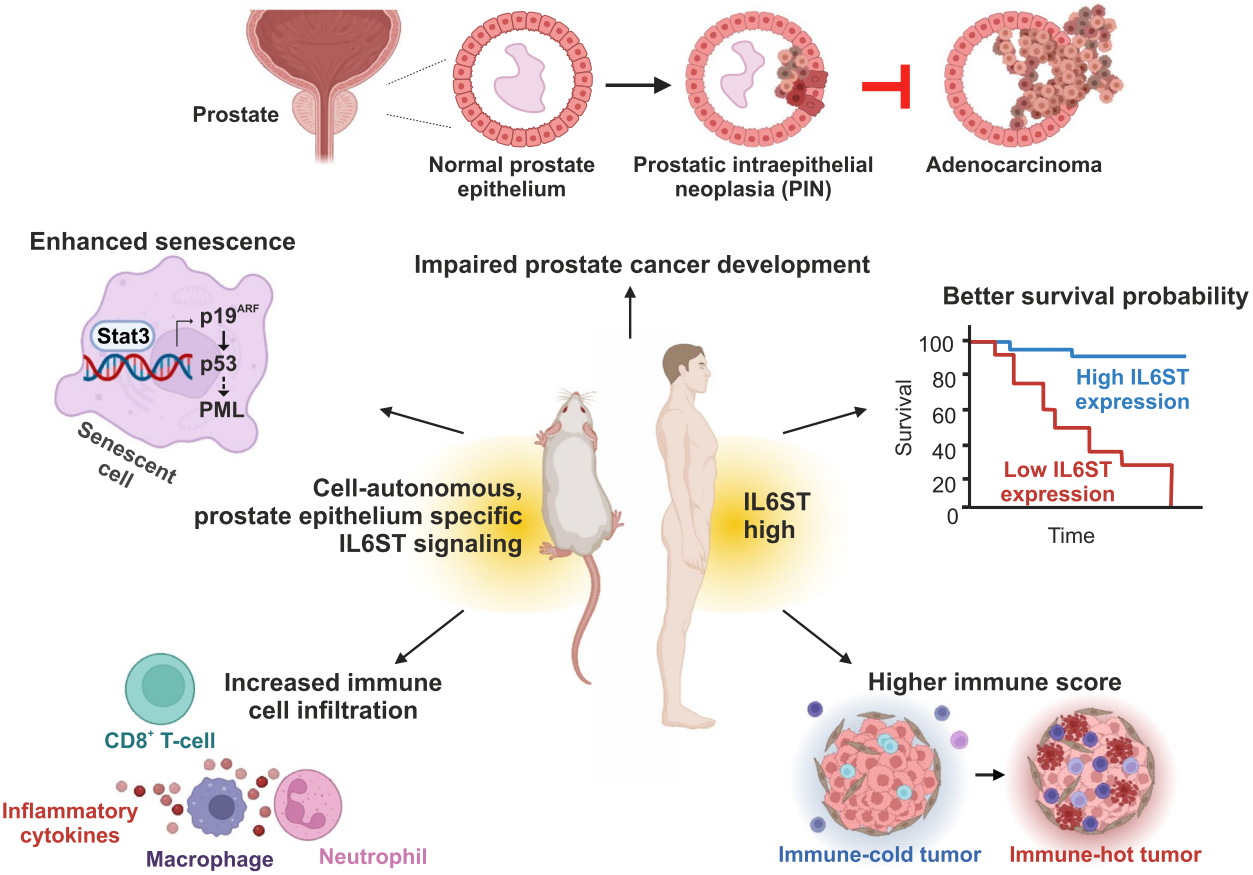

Fig. 7 Proposed roles of active IL6ST signaling in prostate tumorigenesis. Using the genetic mouse model, we showed that cell-autonomous, prostate epithelium-specific and constitutively active IL6ST signaling reduces *Pten*-deficient tumor growth, enhances the STAT3/p19^{ARF}/p53-driven senescence and recruits tumor-infiltrating immune cells (T-cells, neutrophils, and macrophages). In human PCa, high *IL6ST* expression causes active STAT3 signaling, correlates with better survival and is associated with higher level of immune infiltrates

of immune response-related gene sets (Fig. 6a). Furthermore, the top 20 GO-BP gene sets associated with T-cell activation and cytotoxicity, neutrophils and macrophages were upregulated in *IL6ST*^{high} compared to *IL6ST*^{low} expressing patients from the TCGA-PRAD data set, emphasizing the relevance of T-cell, neutrophil and macrophage mediated tumor-defense in PCa patients with high *IL6ST* expression (Fig. 6e). In summary, our data reveal that PCa patients with high *IL6ST* expression exhibit increased senescence, reduced cell cycle activity, and enhanced immune cell infiltration, which likely contribute to their improved survival outcomes.

Discussion

In this study, we show that in a *Pten*-deficient PCa mouse model engineered to constitutively activate IL6ST signaling, STAT3 activation was increased, STAT3 target gene signature was amplified and PCa tumor growth was significantly reduced compared to mice only deficient in *Pten*. The proposed roles of active IL6ST signaling in PCa observed in this study are summarized in Fig. 7. We found that enhanced STAT3 signaling was associated with more pronounced p19^{ARF}/p53 mediated cellular senescence in the tumor tissue. These findings complement previous data showing that inducing a *Stat3* knock out (KO) in PCa mice resulted in larger tumor sizes mediated by loss of senescence [7, 8]. The STAT3 signaling axis thus appears to regulate tumor growth in PCa by primarily inhibiting tumor progression rather than initiation. This is evidenced by the majority of *Pten*$^{peΔ/Δ}$;*L-gp130*$^{peKI/KI}$ mice displaying PINs and not PCa, as was predominantly found in *Pten*$^{peΔ/Δ}$ mice.

The data presented here provide substantial validation and significantly broaden the scope of our previously posited hypotheses [8], that 1) the STAT3/p19^{ARF} axis acts as a safeguard mechanism against malignant progression in PCa, 2) expression levels of constituents of the IL6ST/STAT3 signaling axis could act as key markers to stratify PCa cases into low- and high-risk groups, and

3) strategies aimed at manipulating this signaling pathway could serve as a novel therapeutic approach for PCa treatment.

The tumor-suppressive role of STAT3 signaling in PCa contrasts with the oncogenic function in numerous cancers, where it is often hyperactivated [4, 60]. However, accumulating evidence suggests that it may also function as tumor suppressor depending on signaling context and tumor type [61, 62]. For example, *Stat3* deletion resulted in increased astrocyte tumor formation in SCID mice in the absence but not in the presence of PTEN [63]. Additionally, in a mouse model of colorectal cancer crossed with *Stat3* conditional KO mice, *Stat3* KO in intestinal cells revealed an oncogenic role, whereas a KO during tumor progression enhanced tumor invasiveness, reflecting a tumor suppressive role [64]. In a more specific example, a mouse model of drug-induced cancer demonstrated that STAT3 expression appeared to suppress tumor formation in the presence of a toxicant causing chronic liver injury, inflammation, and fibrosis, whereas it enhanced tumor formation induced by a DNA damaging agent [65]. Further examples have been reported for lung cancer, thyroid cancer and head and neck squamous cell cancers [62], additionally supporting the notion that STAT3 signaling has a dual role, rather than a strictly oncogenic one.

As a possible molecular mechanism underlying this ambiguous behavior, activity of the STAT3β isoform has been suggested. This isoform lacks the C-terminal transactivation domain and was shown to inhibit proliferation and stimulate cell death, possibly through heterodimerizing with STAT3α, thereby preventing it from activating its target genes [61]. In contrast, our data suggest that a different mechanism mediates the tumor suppressive activity of STAT3 signaling in prostate cells with constitutively activated IL6ST. This assumption is based on the observed clear upregulation of transcription in both the absence and presence of PTEN (*Pten*$^{peΔ/Δ}$;*L-gp130*$^{peKI/KI}$ and *L-gp130*$^{peKI/KI}$ mice), as determined from differential gene expression analyses. Another aspect where context dependency seems to be decisive is senescence and its associated SASP. Both have nuanced roles in PCa, with outcomes potentially shaped by context and genetic backgrounds [66]. Examining the transcriptome upon constitutively active IL6ST signaling in greater detail, we identified a significant upregulation of the senescence-associated p19^{ARF}/p53 pathway and PICS. Targeting senescence in this context has been suggested to potentially hold significant promise in cancer therapy [52, 67, 68]. However, a tumor-promoting effect linked to increased SASP in a PCa mouse model with additional KO of *Stat3* has been reported [69]. One possible factor contributing to this divergence in outcomes might be influenced by the specific *Stat3* KO approach that targets only the tyrosine phosphorylation site of *Stat3* and not the DNA-binding domain [70]. Variations in STAT3 expression, such as dominant-negative STAT3, can have profound implications on disease outcomes [71]. Our studies, spanning four independent mouse model systems addressing the IL-6/IL6ST/JAK2/STAT3 signaling axis, consistently indicate a tumor-suppressive effect of STAT3 activation [7, 8]. Specifically, our genetic PCa mouse model with KO of *Stat3*, in which the DNA-binding domain of *Stat3* is targeted [72], leads to aggressive PCa growth [8]. Additionally, we have previously shown that the KO of *Il6*, the activator of the IL6ST/STAT3 signaling, enhances PCa development [8]. By using an independent mouse model, our current study additionally emphasizes a tumor-suppressive role for constitutively active IL6ST/STAT3 signaling and its associated elevated SASP. This divergence in findings highlights the need to consider context- and patient-specific factors, further challenging the current discussion on the therapeutic advantages or hazards of IL-6/STAT3 inhibition.

To assess the potential clinical relevance of our murine findings, we analyzed several PCa patient cohorts. We discovered that in the overall patient population *IL6ST* expression was significantly reduced in the prostate tumor tissue compared to surrounding non-cancerous tissue. However, when we separated these patients into a high and a low *IL6ST* expressing group, we detected that higher *IL6ST* expression correlated with higher *STAT3* expression and, more importantly, with prolonged survival of these patients. Therefore, based on the hypothesis that enhanced IL6ST signaling, as observed in our mouse model, helps restrain cancer progression, we propose that *IL6ST* expression levels, possibly along with *STAT3* and *ARF* levels, could serve as indicators for low- and high-risk PCa groups. However, it must be considered that the chosen RNA analysis methods can impact the outcome [73]. Therefore, further analyses are needed to validate IL6ST expression as a prognostic marker in PCa, including protein-level analysis, robust biomarker models, and functional studies. This could help prevent overtreatment and unnecessary reductions in quality of life for PCa patients [74].

A further important potential lead for future treatment of PCa patients derived from our study is the observation that enhanced IL6ST signaling was associated with high-grade immune cell infiltration at the tumor site. This infiltration included $CD3^+$;$CD8^+$ T-cells, neutrophils, and M1-like macrophages that are considered major drivers of anti-tumor immunity [56, 75], and was accompanied by an upregulation of adaptive and innate immune system-related gene sets. In general, PCa cells and those comprising its microenvironment are known

to express and secrete molecules mediating immunosuppression, rendering PCa immune-cold [19] and thus not a good target for otherwise highly efficient immune-based therapies [76]. PCa is also associated with low mutational burden and low immunogenicity [77], and thus little responsiveness to therapies based on immune checkpoint inhibitors [78]. Consequently, the potential to enhance immunogenicity by manipulating IL6ST signaling could present a novel therapeutic approach in PCa therapy.

Our analysis of human patient data sets supports this idea, confirming that, while most PCa patients examined must be regarded as immune-cold (as determined by the ESTIMATE tool [32]) those with high *IL6ST* expression exhibited a better immune score. These patients also showed upregulated gene sets associated with T-cells, neutrophils, and macrophages and, noteworthy, increased senescence-related gene sets. As to the latter, it remains to be shown whether immune cell infiltration is the direct consequence of enhanced IL6ST signaling and the associated senescence induction or its cause [66, 79]. In either case, there is evidence suggesting that a higher number of tumor infiltrating lymphocytes in PCa is associated with better patient outcomes [80]. Considering the immense potential of novel approaches, such as the induction of synthetic cytokine signaling circuits allowing immune cells to overcome immunosuppressive microenvironments and infiltrate immune-excluded solid tumors [81], it appears conceivable that strategies mediating prostate-specific, active IL6ST signaling have potential to effectively attack tumor cells.

Altogether, the present study reveals that increased IL6ST signaling is linked with suppressed tumor growth and amplified STAT3 target gene signatures. Contrary to its oncogenic role in many cancers, IL6ST/STAT3 signaling demonstrated tumor-suppressive activity in the context of PCa, potentially through the upregulation of the senescence-associated $p19^{ARF}$/p53 pathway. Additionally, elevated IL6ST signaling in tumors was linked to increased immune cell infiltration, implying that enhancing IL6ST signaling might be a promising therapeutic strategy for boosting anti-tumor immunity in PCa. Clinical analysis of PCa patients showed a positive correlation between high *IL6ST* expression and longer recurrence-free survival, suggesting that *IL6ST* expression levels could aid in risk stratification.

Conclusions

In conclusion, our study redefines the role of IL6ST/STAT3 signaling in PCa, uncovering its tumor-suppressive effects through senescence and immune cell recruitment. This challenges the traditional view of STAT3 as an oncogene and questions the strategy of inhibiting this pathway for PCa treatment. Advocating for IL6ST activation as a novel therapeutic strategy, we pave the way for innovative cancer therapies that leverage immune system engagement to combat tumors. Our findings position active IL6ST signaling as a crucial element in developing more effective treatments for PCa, highlighting its potential to transform PCa therapy.

Abbreviations

adj. p-value	Adjusted p-value
ARF	Alternative reading frame
AL	Anterior lobe
CAG	Synthetic CMV-Actin-Globin composite promoter
CGP	Chemical and genetic perturbations
CL	Caudal lobe
DE	Differentially expressed
EpCAM	Epithelial cell adhesion molecule
ERK	Extracellular signal-regulated kinase
ESTIMATE	Estimation of STromal and Immune cells in MAlignant Tumor tissues using Expression data
fGSEA	Fast pre-ranked gene set enrichment analysis
fl	Floxed
FFPE	Formalin-fixed paraffin-embedded
FWHM	Full width at half maximum
GP130	Glycoprotein 130 kDa = IL6ST
GO-BP	Gene Ontology Biological Process
H&E	Hematoxylin & eosin
IF	Immunofluorescence
IHC	Immunohistochemistry
IL-6	Interleukin-6
IL-6R	Interleukin-6 receptor
IL6ST	Interleukin-6 cytokine family signal transducer = GP130
JAK	Janus kinase
KEGG	Kyoto Encyclopedia of Genes and Genomes
KI	Knock in
KO	Knock out
L-gp130	Leucine-gp130
MAPK	Mitogen-activated protein kinase
MFI	Mean fluorescence intensity
NES	Normalized enrichment score
OIS	Oncogene-induced senescence
P	Phospho
PB	Probasin
PCa	Prostate cancer
PCR	Polymerase chain reaction
Pe	Prostate epithelium
PICS	PTEN-loss induced cellular senescence
PIN	Prostatic intraepithelial neoplasia
PI3K	Phosphatidylinositol 3-kinase
PML	Promyelocytic leukemia protein
PTEN	Phosphatase and tensin homolog
qRT-PCR	Quantitative reverse transcription-polymerase chain reaction
RNA-Seq	RNA sequencing
SASP	Senescence-associated secretory phenotype
SD	Standard deviation
SHP2	Src homology 2 domain-containing tyrosine phosphatase-2
ssGSVA	Single sample gene set variation analysis
STAT3	Signal transducer and activator of transcription 3
T	Total
TCGA-PRAD	The Cancer Genome Atlas-PRostate ADenocarcinoma
TME	Tumor microenvironment
VST	Variance stabilizing transformation
WP	WikiPathways
ZSGreen	Zoanthus sp. green fluorescent protein

Supplementary Information

The online version contains supplementary material available at https://doi.org/10.1186/s12943-024-02114-8.

Additional File 1: Supplementary tables.

Additional File 2: Detailed histopathological analysis of mouse prostate lobes 1.

Additional File 3: Detailed histopathological analysis of mouse prostate lobes 2.

Additional File 4: Supplementary methods.

Additional File 5: Supplementary figures and figure legend.

Additional File 6: Flow cytometry gating strategy.

Acknowledgements
We acknowledge the Core Facility Bioinformatics supported by the NCMG research infrastructure (LM2023067 funded by MEYS CR) for their support with the bioinformatic analysis of the RNA sequencing data presented in this paper. This research was supported using resources of the VetCore Facility (VetImaging) of the University of Veterinary Medicine Vienna. The authors are grateful to Dr. Natalie Bordag (Medical University of Graz) for providing help with R programming and bioinformatic analysis, and to Anton Jäger (Medical University of Vienna) for his assistance in generating macroscopic pictures and graphical illustrations. Scientific coaching to C.S. was provided by Gerhard Krumschnabel (medical-writing.at) and was funded by University of Veterinary Medicine Vienna. We acknowledge the use of BioRender.com for creating Fig. 1a, Fig. 4j and Fig. 7.

Authors' contributions
Conceptualization and design: C.S., S.R.-J., L.K.; Development of methodology: C.S., M.R., T.L., K.T., J.K., D.Z., M.O., F.S., S.H., S.L., S.R.-J.; Acquisition of data: C.S., M.R., T.L., K.T., D.L., M.S., R.Z., J.K., S.S., S.D., D.Z., H.A.N., M.O., T.R., F.S.; Technical assistance: M.S., P.K., J.Y., B.T., M.T., N.S.H., S.T.; Project administration: C.S., S.R.-J., L.K.; Formal analysis: C.S., M.R., K.T., V.H., F.S.; Analysis and interpretation of data: C.S., T.L., H.A.N., F.S., S.H., S.L., S.R.-J., L.K.; Resources: C.S., J.P., V.B., J.L.P., G.E., S.P., R.E., P.W., S.R.-J., L.K.; Study supervision: S.R.-J., L.K.; Funding acquisition: S.R.-J., L.K.; Writing—original draft: C.S.; Figure preparation: C.S., M.R., M.S., F.S.; Writing—review & editing: C.S., M.R., T.L., K.T., H.A.N., S.S., S.D., M.O., T.R., P.W., F.S., S.H., S.L., S.R.-J., L.K.; All authors read and approved the final manuscript.

Authors' information
Not applicable.

Funding
This study was financially supported by grant Nr. 70112589 from the Deutsche Krebshilfe, Bonn, Germany to S.R.-J. L.K. acknowledges the support from MicroONE, a COMET Modul under the lead of CBmed GmbH, which is funded by the federal ministries BMK and BMDW, the provinces of Styria and Vienna, and managed by the Austrian Research Promotion Agency (FFG) within the COMET-Competence Centers for Excellent Technologies-program. Financial support was also received from the Austrian Federal Ministry of Science, Research and Economy, the National Foundation for Research, Technology and Development, the Christian Doppler Research Association and Siemens Healthineers. L.K. was also supported by European Union Horizon 2020 Marie Sklodowska-Curie Doctoral Network grants (ALKATRAS, n. 675712; FANTOM, n. P101072735 and eRaDicate, n. 101119427) as well as BM Fonds (n. 15142), the Margaretha Hehberger Stiftung (n. 15142), the Christian Doppler Lab for Applied Metabolomics (CDL-AM), and the Austrian Science Fund (FWF) P26011, P29251 and P34781. This work was also supported by the Austrian Science Fund (FWF) W1241 to P.W., the Austrian Science Fund (FWF) DOC 59–833 "International PhD Program in Translational Oncology – IPPTO" to R.E. and L.K., the Austrian Science Fund (FWF) P35069-B "CDHR5 in Intestinal Barrier Function and Inflammation" to R.E. and the Austrian Science Fund (FWF) P32771 to J.K. and G.E. Additionally, this research was funded by the Vienna Science and Technology Fund (WWTF), grant number LS19-018. L.K. is a member of the European Research Initiative for ALK-Related Malignancies (www.erialcl.net). The National Institute for Cancer Research (Programme EXCELES, No. LX22NPO5102) funded by Next Generation EU is gratefully acknowledged for funding.

Availability of data and materials
The RNA-Seq data set supporting the conclusions of this article is publicly available in the GEO repository with the accession number GSE277063. The following publicly available data sets were used: TCGA-PRAD [28], MSKCC Prostate GSE21032 [44], SMD GSE40272 [45] and data sets provided by the Oncomine™ Research Premium Edition database [42] and by MSigDB [35].

Declarations

Ethics approval and consent to participate
Animal experiments and care were conducted in accordance with the guidelines of institutional authorities and approved by the Federal Ministry of Austria for Education, Science and Research (BMWFW-66.009/0307-WF/V/3b/2017 and the associated amendments).

Consent for publication
Not applicable.

Competing interests
The authors declare no competing interests.

Author details
[1]Department of Pathology, Medical University of Vienna, Vienna, Austria. [2]Biochemical Institute, University of Kiel, Kiel, Germany. [3]Unit of Laboratory Animal Pathology, University of Veterinary Medicine Vienna, Vienna, Austria. [4]Department of Biomedical Imaging and Image-Guided Therapy, Division of Nuclear Medicine, Medical University of Vienna, Vienna, Austria. [5]Center for Biomarker Research in Medicine GmbH (CBmed), Graz, Styria, Austria. [6]Central European Institute of Technology, Masaryk University, Brno, Czech Republic. [7]Christian Doppler Laboratory for Applied Metabolomics, Medical University of Vienna, Vienna, Austria. [8]Department of Dermatology and Venereology, Medical University of Graz, Graz, Austria. [9]Center for Cancer Research, Medical University of Vienna & Comprehensive Cancer Center, Vienna, Austria. [10]Institute of Animal Breeding and Genetics, University of Veterinary Medicine Vienna, Vienna, Austria. [11]Department of Molecular Biology, Umeå University, Umeå, Sweden. [12]Department of Biomedical Sciences, Malmö Universitet, Malmö, Sweden. [13]Comprehensive Cancer Center, Medical University of Vienna, Vienna, Austria. [14]BioTechMed Graz, Graz, Austria. [15]Department of Nutritional Sciences, Faculty of Life Sciences, University of Vienna, Vienna, Austria. [16]Department of Biological Sciences and Pathobiology, Physiology and Biophysics, University of Veterinary Medicine Vienna, Vienna, Austria. [17]Department of Cell Biology, Charles University, Prague, Czech Republic and Biotechnology and Biomedicine Centre of the Academy of Sciences and Charles University (BIOCEV), Vestec u Prahy, Czech Republic. [18]Institute of Medical Biochemistry, University of Veterinary Medicine Vienna, Vienna, Austria.

Received: 17 March 2024 Accepted: 5 September 2024
Published online: 31 October 2024

References

1. Wang L, Lu B, He M, Wang Y, Wang Z, Du L. Prostate Cancer Incidence and Mortality: Global Status and Temporal Trends in 89 Countries From 2000 to 2019. Front Public Health. 2022;10:176.
2. del Pino-Sedeño T, Infante-Ventura D, de Armas CA, de Pablos-Rodríguez P, Rueda-Domínguez A, Serrano-Aguilar P, Trujillo-Martín MM. Molecular Biomarkers for the Detection of Clinically Significant Prostate Cancer: A Systematic Review and Meta-analysis. Eur Urol Open Sci. 2022;46:105–27.
3. Scherger AK, Al-Maarri M, Maurer HC, et al. Activated gp130 signaling selectively targets B cell differentiation to induce mature lymphoma and plasmacytoma. JCI Insight. 2019;4:e128435–e128435.
4. Golus M, Bugajski P, Chorbińska J, Krajewski W, Lemiński A, Saczko J, Kulbacka J, Szydełko T, Małkiewicz B. STAT3 and Its Pathways' Dysregulation-Underestimated Role in Urological Tumors. Cells. 2022;11:3024.

5. Mora LB, Buettner R, Seigne J, et al. Constitutive activation of Stat3 in human prostate tumors and cell lines: Direct inhibition of Stat3 signaling induces apoptosis of prostate cancer cells. Cancer Res. 2002;62:6659–66.
6. Lee H, Jeong AJ, Ye SK. Highlighted STAT3 as a potential drug target for cancer therapy. BMB Rep. 2019;52:415–23.
7. Pencik J, Philippe C, Schlederer M, et al. STAT3/LKB1 controls metastatic prostate cancer by regulating mTORC1/CREB pathway. Mol Cancer. 2023;22:133.
8. Pencik J, Schlederer M, Gruber W, et al. STAT3 regulated ARF expression suppresses prostate cancer metastasis. Nat Commun. 2015;6:7736–8802.
9. Schaper F, Rose-John S. Interleukin-6: Biology, signaling and strategies of blockade. Cytokine Growth Factor Rev. 2015;26:475–87.
10. Liu Z, Zhao Y, Fang J, Cui R, Xiao Y, Xu Q. SHP2 negatively regulates HLA-ABC and PD-L1 expression via STAT1 phosphorylation in prostate cancer cells. Oncotarget. 2017;8:53518–30.
11. Chen H, Zhou L, Wu X, Li R, Wen J, Sha J, Wen X. The PI3K/AKT pathway in the pathogenesis of prostate cancer. Front Biosci - Landmark. 2016;21:1084–91.
12. Sheng X, Bin LW, Wang DL, Chen KH, Cao JJ, Luo Z, He J, Li MC, Liu WJ, Yu C. YAP is closely correlated with castration-resistant prostate cancer, and downregulation of YAP reduces proliferation and induces apoptosis of PC-3 cells. Mol Med Rep. 2015;12:4867–76.
13. Jamaspishvili T, Berman DM, Ross AE, Scher HI, De Marzo AM, Squire JA. Lotan TL (2018) Clinical implications of PTEN loss in prostate cancer. Nat Rev Urol. 2018;15(4):222–34.
14. Choudhury AD. PTEN-PI3K pathway alterations in advanced prostate cancer and clinical implications. Prostate. 2022;82(Suppl 1):S60–72.
15. Chen Z, Trotman LC, Shaffer D, et al. Crucial role of p53-dependent cellular senescence in suppression of Pten-deficient tumorigenesis. Nature. 2005;436:725–30.
16. Parisotto M, Grelet E, El Bizri R, Metzger D. Senescence controls prostatic neoplasia driven by Pten loss. Mol Cell Oncol. 2019;6:1511205.
17. Young ARJ, Narita M. SASP reflects senescence. EMBO Rep. 2009;10:228–30.
18. Huang W, Hickson LTJ, Eirin A, Kirkland JL, Lerman LO. Cellular senescence: the good, the bad and the unknown. Nat Rev Nephrol. 2022;18:611–27.
19. Stultz J, Fong L. How to turn up the heat on the cold immune microenvironment of metastatic prostate cancer. Prostate Cancer Prostatic Dis. 2021;24:697–717.
20. Suzuki A, Yamaguchi MT, Ohteki T, et al. T cell-specific loss of Pten leads to defects in central and peripheral tolerance. Immunity. 2001;14:523–34.
21. Wu X, Wu J, Huang J, Powell WC, Zhang JF, Matusik RJ, Sangiorgi FO, Maxson RE, Sucov HM, Roy-Burman P. Generation of a prostate epithelial cell-specific Cre transgenic mouse model for tissue-specific gene ablation. Mech Dev. 2001;101:61–9.
22. Limberger T, Schlederer M, Trachtová K, et al. KMT2C methyltransferase domain regulated INK4A expression suppresses prostate cancer metastasis. Mol Cancer. 2022;21:1–19.
23. Birbach A, Eisenbarth D, Kozakowski N, Ladenhauf E, Schmidt-Supprian M, Schmid JA. Persistent inflammation leads to proliferative neoplasia and loss of smooth muscle cells in a prostate tumor model. Neoplasia. 2011;13:692–703.
24. Redmer T, Raigel M, Sternberg C, et al. JUN mediates the senescence associated secretory phenotype and immune cell recruitment to prevent prostate cancer progression. Mol Cancer. 2024;23:114.
25. Schmidt U, Weigert M, Broaddus C, Myers G (2018) Cell Detection with Star-Convex Polygons. In: Frangi A., Schnabel J., Davatzikos C., Alberola-López C., Fichtinger G. (eds) Medical Image Computing and Computer Assisted Intervention – MICCAI 2018. Lecture Notes in Computer Science, vol 11071. Springer, Cham. p. 265–273. https://link.springer.com/chapter/10.1007/978-3-030-00934-2_30.
26. Ding Z, Wu CJ, Chu GC, et al. SMAD4-dependent barrier constrains prostate cancer growth and metastatic progression. Nature. 2011;470:269–76.
27. Drost J, Karthaus WR, Gao D, Driehuis E, Sawyers CL, Chen Y, Clevers H. Organoid culture systems for prostate epithelial and cancer tissue. Nat Protoc. 2016;11:347–58.
28. Abeshouse A, Ahn J, Akbani R, et al. The Molecular Taxonomy of Primary Prostate Cancer. Cell. 2015;163:1011–25.
29. Gao J, Aksoy BA, Dogrusoz U, et al. Integrative analysis of complex cancer genomics and clinical profiles using the cBioPortal. Sci Signal. 2013;6:1.
30. Cerami E, Gao J, Dogrusoz U, et al. The cBio cancer genomics portal: an open platform for exploring multidimensional cancer genomics data. Cancer Discov. 2012;2:401–4.
31. CRAN - Package survminer. https://cran.r-project.org/web/packages/survminer/index.html. Accessed 9 Feb 2023.
32. Yoshihara K, Shahmoradgoli M, Martínez E, et al. Inferring tumour purity and stromal and immune cell admixture from expression data. Nat Commun. 2013;4:2612.
33. Stuhlmann-Laeisz C, Lang S, Chalaris A, et al. Forced dimerization of gp130 leads to constitutive STAT3 activation, cytokine-independent growth, and blockade of differentiation of embryonic stem cells. Mol Biol Cell. 2006;17:2986–95.
34. Wang S, Gao J, Lei Q, et al. Prostate-specific deletion of the murine Pten tumor suppressor gene leads to metastatic prostate cancer. Cancer Cell. 2003;4(3):209–21.
35. Subramanian A, Tamayo P, Mootha VK, et al. Gene set enrichment analysis: A knowledge-based approach for interpreting genome-wide expression profiles. Proc Natl Acad Sci U S A. 2005;102:15545–50.
36. Liberzon A, Birger C, Thorvaldsdóttir H, Ghandi M, Mesirov JP, Tamayo P. The Molecular Signatures Database (MSigDB) hallmark gene set collection. Cell Syst. 2015;1:417.
37. Swoboda A, Soukup R, Eckel O, et al. STAT3 promotes melanoma metastasis by CEBP-induced repression of the MITF pathway. Oncogene. 2021;40:1091–105.
38. Azare J, Leslie K, Al-Ahmadie H, Gerald W, Weinreb PH, Violette SM, Bromberg J. Constitutively activated Stat3 induces tumorigenesis and enhances cell motility of prostate epithelial cells through integrin beta 6. Mol Cell Biol. 2007;27:4444–53.
39. Carpenter RL, Lo HW. STAT3 Target Genes Relevant to Human Cancers. Cancers (Basel). 2014;6:897–925.
40. Darnell JE. Kerr Ian M, Stark GR (1994) Jak-STAT Pathways and Transcriptional Activation in Response to IFNs and Other Extracellular Signaling Proteins. Science. 1979;264:1415–21.
41. Wen Z, Zhong Z, Darnell JE. Maximal Activation of Transcription by Statl and Stat3 Requires Both Tyrosine and Serine Phosphorylation. Cell. 1995;82:241–50.
42. Rhodes DR, Yu J, Shanker K, Deshpande N, Varambally R, Ghosh D, Barrette T, Pandey A, Chinnaiyan AM. ONCOMINE: a cancer microarray database and integrated data-mining platform. Neoplasia. 2004;6:1–6.
43. Aguirre-Gamboa R, Gomez-Rueda H, Martínez-Ledesma E, Martínez-Torteya A, Chacolla-Huaringa R, Rodriguez-Barrientos A, Tamez-Peña JG, Treviño V. SurvExpress: an online biomarker validation tool and database for cancer gene expression data using survival analysis. PLoS ONE. 2013;8:e74250.
44. Taylor BS, Schultz N, Hieronymus H, et al. Integrative Genomic Profiling of Human Prostate Cancer. Cancer Cell. 2010;18:11–22.
45. Gulzar ZG, Mckenney JK, Brooks JD. Increased expression of NuSAP in recurrent prostate cancer is mediated by E2F1. Oncogene. 2013;32:70–7.
46. Tan MH, Li J, Xu HE, Melcher K, Yong EL. Androgen receptor: structure, role in prostate cancer and drug discovery. Acta Pharmacol Sin. 2015;36:3–23. https://doi.org/10.1038/aps.2014.18. https://www.nature.com/articles/aps201418#citeas.
47. Oberhuber M, Pecoraro M, Rusz M, et al (2020) STAT3-dependent analysis reveals PDK4 as independent predictor of recurrence in prostate cancer. Mol Syst Biol. https://doi.org/10.15252/MSB.20199247
48. Wiebringhaus R, Pecoraro M, Neubauer HA, et al. Proteomic analysis identifies ndufs1 and atp5o as novel markers for survival outcome in prostate cancer. Cancers (Basel). 2021;13:6036.
49. Kiuchi N, Nakajima K, Ichiba M, Fukada T, Narimatsu M, Mizuno K, Hibi M, Hirano T. STAT3 Is Required for the gp130-mediated Full Activation of the c-myc Gene. J Exp Med. 1999;189:63–73.
50. Johnson DE, O'Keefe RA, Grandis JR. Targeting the IL-6/JAK/STAT3 signalling axis in cancer. Nat Rev Clin Oncol. 2018;15(4):234–48.
51. Hanahan D. Hallmarks of Cancer: New Dimensions. Cancer Discov. 2022;12:31–46.
52. Alimonti A, Nardella C, Chen Z, et al. A novel type of cellular senescence that can be enhanced in mouse models and human tumor xenografts to suppress prostate tumorigenesis. J Clin Invest. 2010;120:681–93.
53. Bischof O, Kirsh O, Pearson M, Itahana K, Pelicci PG, Dejean A. Deconstructing PML-induced premature senescence. EMBO J. 2002;21:3358–69.

54. Guccini I, Revandkar A, D'Ambrosio M, et al. Senescence Reprogramming by TIMP1 Deficiency Promotes Prostate Cancer Metastasis. Cancer Cell. 2021;39:68–82.e9.
55. Ouelle DE, Zindy F, Ashmun RA, Sherr CJ. Alternative reading frames of the INK4a tumor suppressor gene encode two unrelated proteins capable of inducing cell cycle arrest. Cell. 1995;83:993–1000.
56. Reiser J, Banerjee A. Effector, Memory, and Dysfunctional CD8(+) T Cell Fates in the Antitumor Immune Response. J Immunol Res. 2016. https://doi.org/10.1155/2016/8941260.
57. Jorgovanovic D, Song M, Wang L, Zhang Y. Roles of IFN-γ in tumor progression and regression: a review. Biomark Res. 2020;8:49. https://doi.org/10.1186/s40364-020-00228-x.
58. Farhood B, Najafi M, Mortezaee K. CD8+ cytotoxic T lymphocytes in cancer immunotherapy: A review. J Cell Physiol. 2019;234:8509–21.
59. Sun W, Shi H, Yuan Z, Xia L, Xiang X, Quan X, Shi W, Jiang L. Prognostic Value of Genes and Immune Infiltration in Prostate Tumor Microenvironment. Front Oncol. 2020. https://doi.org/10.3389/FONC.2020.584055/FULL.
60. Tošić I, Frank DA. STAT3 as a mediator of oncogenic cellular metabolism: Pathogenic and therapeutic implications. Neoplasia. 2021;23:1167–78.
61. Zhang HF, Lai R. STAT3 in cancer-friend or foe? Cancers (Basel). 2014;6:1408–40.
62. Tolomeo M, Cascio A. The Multifaced Role of STAT3 in Cancer and Its Implication for Anticancer Therapy. Int J Mol Sci. 2021;22:603.
63. De La Iglesia N, Konopka G, Puram SV, Chan JA, Bachoo RM, You MJ, Levy DE, DePinho RA, Bonni A. Identification of a PTEN-regulated STAT3 brain tumor suppressor pathway. Genes Dev. 2008;22:449–62.
64. Musteanu M, Blaas L, Mair M, et al. Stat3 is a negative regulator of intestinal tumor progression in Apc(Min) mice. Gastroenterology. 2010. https://doi.org/10.1053/J.GASTRO.2009.11.049.
65. Wang H, Lafdil F, Wang L, Park O, Yin S, Niu J, Miller AM, Sun Z, Gao B. Hepatoprotective versus oncogenic functions of STAT3 in liver tumorigenesis. Am J Pathol. 2011;179:714–24.
66. Schmitt CA, Wang B, Demaria M. Senescence and cancer — role and therapeutic opportunities. Nat Rev Clin Oncol. 2022;19:619–36.
67. Rufini A, Tucci P, Celardo I, Melino G. Senescence and aging: the critical roles of p53. Oncogene. 2013;32:5129–43. https://doi.org/10.1038/onc.2012.640.
68. Bousset L, Gil J. Targeting senescence as an anticancer therapy. Mol Oncol. 2022;16:3855–80.
69. Toso A, Revandkar A, DiMitri D, et al. Enhancing chemotherapy efficacy in Pten-deficient prostate tumors by activating the senescence-associated antitumor immunity. Cell Rep. 2014;9:75–89.
70. Takeda K, Kaisho T, Yoshida N, Takeda J, Kishimoto T, Akira S. Stat3 activation is responsible for IL-6-dependent T cell proliferation through preventing apoptosis: generation and characterization of T cell-specific Stat3-deficient mice. J Immunol. 1998;161(9):4652–60. Erratum in: J Immunol. 2015;194(7):3526. https://doi.org/10.4049/jimmunol.1500168. https://pubmed.ncbi.nlm.nih.gov/9794394/.
71. Minegishi Y, Saito M, Tsuchiya S, et al. Dominant-negative mutations in the DNA-binding domain of STAT3 cause hyper-IgE syndrome. Nature. 2007;448:1058–62.
72. Alonzi T, Maritano D, Gorgoni B, Rizzuto G, Libert C, Poli V. Essential Role of STAT3 in the Control of the Acute-Phase Response as Revealed by Inducible Gene Activation in the Liver. Mol Cell Biol. 2001;21:1621–32.
73. Kremer A, Kremer T, Kristiansen G, Tolkach Y. Where is the limit of prostate cancer biomarker research? Systematic investigation of potential prognostic and diagnostic biomarkers. BMC Urol. 2019;19:46.
74. Loeb S, Bjurlin MA, Nicholson J, Tammela TL, Penson DF, Carter HB, Carroll P, Etzioni R. Overdiagnosis and overtreatment of prostate cancer. Eur Urol. 2014;65:1046–55.
75. Russo M, Nastasi C. Targeting the Tumor Microenvironment: A Close Up of Tumor-Associated Macrophages and Neutrophils. Front Oncol. 2022. https://doi.org/10.3389/fonc.2022.871513.
76. Strasner A, Karin M. Immune infiltration and prostate cancer. Front Oncol. 2015;5:128.
77. Wang L, Pan S, Zhu B, Yu Z, Wang W. Comprehensive analysis of tumour mutational burden and its clinical significance in prostate cancer. BMC Urol. 2021;21:1–10.
78. Maleki Vareki S. High and low mutational burden tumors versus immunologically hot and cold tumors and response to immune checkpoint inhibitors. J Immunother Cancer. 2018;6:157.
79. Reimann M, Schrezenmeier J, Richter-Pechanska P, et al. Adaptive T-cell immunity controls senescence-prone MyD88- or CARD11-mutant B-cell lymphomas. Blood. 2021;137:2785–99.
80. Miyake M, Hori S, Owari T, Oda Y, Tatsumi Y, Nakai Y, Fujii T, Fujimoto K. Clinical Impact of Tumor-Infiltrating Lymphocytes and PD-L1-Positive Cells as Prognostic and Predictive Biomarkers in Urological Malignancies and Retroperitoneal Sarcoma. Cancers (Basel). 2020;12:1–28.
81. Allen GM, Frankel NW, Reddy NR, Bhargava HK, Yoshida MA, Stark SR, Purl M, Lee J, Yee JL, Yu W, Li AW, Garcia KC, El-Samad H, Roybal KT, Spitzer MH, Lim WA. Synthetic cytokine circuits that drive T cells into immune-excluded tumors. Science. 2022;378(6625):eaba1624. https://doi.org/10.1126/science.aba1624.

Publisher's Note

Springer Nature remains neutral with regard to jurisdictional claims in published maps and institutional affiliations.